Università degli Studi di Padova

Dipartimento di Fisica e Astronomia

Corso di Laurea Magistrale in Fisica

Collective Behaviour of Active Binary Particle Mixtures

Laureando:
Federico Gnesotto

Matricola:
1079233

Relatore:
Prof. Enzo Orlandini

Relatore estero:
Prof. Erwin Frey

Anno Accademico 2015-2016

To my uncle
Roberto

It can scarcely be denied that the supreme goal of all theory is to make the irreducible basic elements as simple and as few as possible without having to surrender the adequate representation of a single datum of experience.

Albert Einstein, 1933

Riassunto

Il lavoro di Tesi si è svolto nell'ambito della fisica dei sistemi attivi e più in generale dei sistemi complessi. Motivati dal crescente numero di esperimenti e simulazioni di tali sistemi, abbiamo intrapreso lo studio di sistemi binari di particelle attive. In particolare, abbiamo fatto uso dell'equazione di Boltzmann per sistemi non in equilibrio: le due specie analizzate sono contraddistinte da diverse densità e diverso rumore stocastico. Abbiamo inoltre ipotizzato che sia per le interazioni tra particelle della stessa specie, che per quelle appartententi a due specie diverse, la regola di collisione fosse di tipo polare.

Dopo aver ricavato le equazioni del moto che governano il sistema binario, le abbiamo linearizzate attorno all'ovvia soluzione corrispondente ad una fase isotropa ed omogenea. La scelta del sistema autovalore-autovettore adatto a descrivere una miscela di particelle polari, ci ha consentito di ricavare il diagramma di fase e di evidenziare altresì le sue peculiarità.

Considerando termini fino al terz'ordine nelle equazioni del moto, siamo stati in grado di ricavare le equazioni nonlineari dell'Idrodinamica che governano tale sistema. Vista l'impossibilità di risolverle analiticamente, abbiamo suggerito alcune possibili implicazioni di queste e auspichiamo che una futura analisi più dettagliata possa portare a maggiori risultati.

Abbiamo infine utilizzato un algoritmo numerico (SNAKE) per risolvere l'Equazione di Boltzmann e analizzare le strutture spaziali (patterns) emergenti nel nostro sistema. Ritroviamo le ben note onde di densità, oltre a confermare la suddetta analisi lineare. Anche in questo caso mettiamo in evidenza come il comportamento delle due specie sia fortemente correlato: i diagrammi di fase coincidono e le onde di densità hanno sempre la stessa direzione e velocità; i profili sono tuttavia differenti. Tale comportamento può essere verosimilmente spiegato tenendo conto che ciò che differenzia i due sistemi non sono proprietà spaziali (come potrebbero essere diversa curvatura (chiralità) o velocità), quanto piuttosto proprietà statistiche come il rumore stocastico o di bulk come la densità.

Contents

1 Introduction

1.1 Soft active matter

Entities capable of converting *locally* at particle level, an external energy input into persistent motion are commonly referred to as *active matter* [29, 39]. These units can move by means of molecular motors at cellular level [43, 55], using their cilia and flagella if we think of bacterial suspensions [4, 55] or by fluttering their wings if we look at flocks of birds [45, 50, 51, 55]. Interestingly, even in two-dimensions these systems are able to organize themselves into ordered structures evolving from a disordered state: notably, this wouldn't be possible for an equilibrium system since for the latter the Mermin-Wagner theorem holds [31]. This property makes the study of active matter phenomena even more appealing. This ordered motion of many individuals behaving as one is usually referred to as "flocking". Biologists have been studying why animals flock together for many years now: experiments on locusts, birds, schools of fish have been carried out and have yielded interesting insights into how interactions between the individuals or between an individual an its surroundings work [2, 5, 24, 27, 42]. From a physicist's perspective many questions regarding these systems can arise: are these patterns model-specific or do a few general fundamental rules for collective behaviour exist? How can they be implemented into a physical model? How does this nonequilibrium disorder $\Leftrightarrow$ order transition happen and what are the main differences with an equilibrium one?

Left: Colony of ants forming a bridge-like structure to help other ants reach the leaf. *Center:* A school of fish organizes into a toroidal shape in order to confuse predators. *Right:* Birds flying in a complex butterfly-shaped flock in the sky above Rome.

The great success of this research field in physics is mostly due to the fact that, remarkably, the main properties of flocking can be reproduced by easily-implemented experiments for example on vibrated rods or disks [14, 15, 57] and that very simple theoretical models of self-propelled units with a few "rules" are capable of reproducing collective behaviour when implemented in simulations. Before describing the first physical model proposed by Vicsek [54], we introduce some general concepts of

active matter theory that will be useful to classify the different phenomena.

Elongated active particles or rods can be divided into two classes, according to their mean direction of motion and their intrinsic symmetries: head-tail asymmetric rods that move in a definite direction with non-zero mean velocity are called *polar*, while head-tail symmetric ones that have zero mean velocity are called *apolar*. A sketch of the two classes is given in Fig. 1.

This self-propelled particles can form different ordered states, among which the most studied in literature are: polar states and nematic states. An illustration of these two possibilities is given in Fig. 2. We would like to stress the difference between the classification of single active units and the possible phases that elongated particles can form: a nematic state can be constituted by both polar and apolar units, while a polar phase is only made up of polar rods.

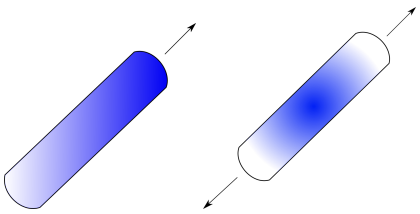

Figure 1: Elongated particles are classified according to their direction of motion and head-tail symmetry. *Left:* polar rod. *Right:* apolar rod.

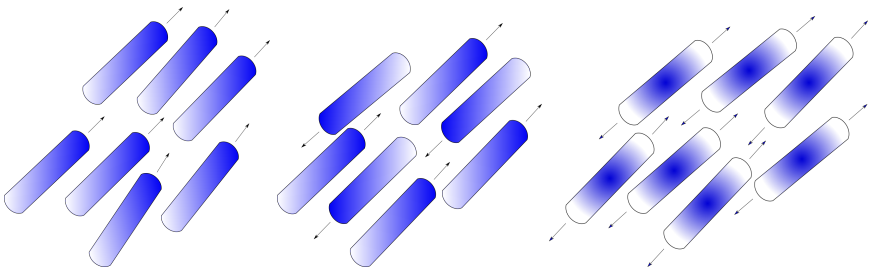

Figure 2: *Left:* Polar order of polar rods. *Center:* Nematic order of polar rods. *Right:* Nematic order of nematic rods.

In real systems, particles move on a substrate (2-D) or they are surrounded by fluid (3-D): depending on the interaction system $\Leftrightarrow$ surroundings an active system is called "dry" if the overall momentum of the particles is *not* conserved. Their motion is overdamped and momentum is dissipated through friction with the substrate: the only conserved quantity is the particle number [57]. For these systems it is a frequently used approximation to neglect the hydrodynamic interactions active particle $\Leftrightarrow$ substrate [21]. The problem is usually further simplified and all particles regarded as moving with constant speed, completely forgetting about their

surroundings. Examples of "dry" systems are suspensions of bacteria on a surface [38, 59], driven actin filaments [43, 44], animals moving on land [50] or vibrated polar disks [14, 56].

Systems in which long-range hydrodynamic interactions *cannot* be neglected are called "wet". A good example of such a system is a population of bacteria swimming in bulk [4, 26, 28].

Now that we have generally defined what exactly these "moving spins" or self-propelled particles (SPPs) are, how their ordered phases look like and how we describe their interaction with the medium, we can be a little bit more precise and re-adapt the concept of *order parameter*, already introduced in the theory of equilibrium phase transitions, to nonequilibrium ones. This helps us to describe in a more mathematical sense what we intuitively regard as ordered and disordered states. Having in mind a system of N active entities equal to one another and moving with the same speed v_0, the order parameter can be defined as [55]

$$\varphi = \frac{1}{N v_0} \sum_{i=1}^{N} \mathbf{v}_i \,. \tag{1.1}$$

The first thing we notice is that this vectorial quantity is dimensionless and its magnitude smaller or equal to one. In particular, the closer it is to one the more "ordered" the phase is, since all particles have roughly the same velocity. Usually the state of a system is determined by one or more *control parameters* that can vary and thus change the configuration of the system (temperature, density etc.).

For its fundamental role in the development of models describing active matter and for being the reference for all our work, we outline the basic features of the Vicsek model (VM) for self propelled particles [54]. All units are equal in shape, have the same speed v_0 and move on a plane. The fundamental "rule" is: at each time step the direction of motion of a particle is determined by the average of the directions of all particles within a certain *interaction radius* r, plus a small noise randomly extracted from a uniform distribution on a predefined interval.

It is interesting to relate this model to an equilibrium one describing a paramagnetic $\Leftrightarrow$ ferromagnetic transition: in a VM aligning spins are replaced by aligning velocities on a plane and random fluctuations due to temperature effects are modelled via uniform noise.

Top: school of fish swimming in a polarized state. *Bottom:* fishes interacting with one another to form a swirl.

The fundamental difference between the two model is that in the VM we deal with "moving spins" that break rotational symmetry via a kinetic non-equilibrium phase transition, whereas in the case of magnetic spins everything is in equilibrium and can be described by a Hamiltonian theory, based on the principle of conservation of energy. It is an intrinsic property of active SPP systems that the order parameter coincides with the *average velocity* (aside from a factor v_0 for dimensions), so that the "spin" of each particle is precisely its velocity [29, 50].

As already remarked, two-dimensional equilibrium systems cannot exhibit flocking, as the Mermin-Wagner theorem [31] prohibits spontaneous breaking of continuous symmetries at finite temperature in systems with dimension $d \leq 2$. Therefore, this kinetic disorder-order transition already reproduced by a simple model like the VM, is an exclusive feature of out-of-equilibrium systems. An explicit proof of this fact by symmetry considerations can be found in [51].

A different approach to active matter is the one proposed by Toner and Tu: their analysis starts directly by writing down the equations of motion for the "slow" (compared to microscopic dynamics) coarse-grained variables *velocity* and *density* [50]. Their equation for the velocity resembles Navier Stokes hydrodynamic equation with a few fundamental differences. What they discover is that the fluctuations in the velocity $\mathbf{v}$ at long wavelengths are suppressed compared to the magnetic case: this leads to an increase of the alignment between individuals and thus renders long-range order. Another phenomenon detected for the first time in systems of elongated rods [34], but already present in simulations of nematic particles [11], are giant number fluctuations (GNF): the fluctuation of the number of self-propelled units in an increasing area of the system scales *linearly* with the number of units in this area [39, 52]. Again this phenomenon is characteristic of out-of-equilibrium systems: equilibrium fluctuations are shown to scale as the square root of the number of particles.

In most SPP models the interactions between the particles are modelled via a *collision rule*: the cartoons of Fig. 3, 4 explain graphically what is meant by *polar* and *antipolar* collision rules. A nematic collision rule is a combination of a polar and an antipolar one (see App. A): if the angle between the two species is smaller than $\pi/2$ the interaction is polar, otherwise antipolar. Particularly important for our purposes is the approach that Bertin *et al.* [6] introduced. They consider a dry system of polar self-propelled particles on a plane, with an explicit polar collision rule (see Fig. 3) and analyse it through a Boltzmann approach, thus retaining only *binary collisions*.

Remarkably, in most physical models for active matter including the ones listed above, the active particles are indistinguishable from one another and all share the same speed. This is a physical simplification that is practically never realized in nature, since heterogeneities are present at different levels in most biological systems.

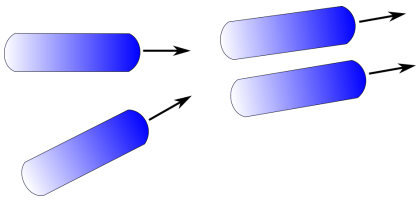

Figure 3: Two polar rods colliding via a polar interaction rule: the direction after the collision is the same and the outgoing angle is assumed to be the average of the two incoming ones (other choices are possible [17]).

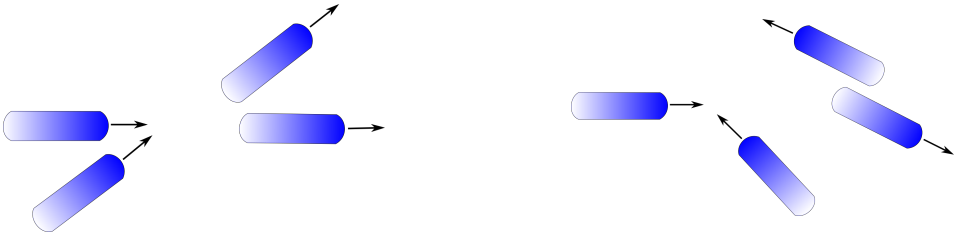

Figure 4: Polar rods colliding with an *antipolar* collision rule: if the angle between the two rods is smaller than some constant Ψ, the two particles don't interact and follow their previous trajectories (left). If the difference of the incoming angles is instead bigger than Ψ, the two particles interact: they exit the collision with opposite directions (right). In our example $\Psi = \pi/2$.

1.2 Binary mixtures of self-propelled particles

In the cytoskeleton [18], as well as in herds of mammals [12] or in schools of fish [33], many species are usually present that differ e.g. in number, in shape, or that move with different speeds. Heterogeneous active systems have not been studied extensively so far, but their relevance is evident both in physics and biology.

In this work, we simplify this problem as much as possible and consider a binary mixture composed of two species of SPPs. We ask ourselves whether a simple difference in their alignment noise or in their density already leads to new interesting collective behaviours.

To be explicit, the main questions that we ask are:

1. We know that in single species we observe an order $\Leftrightarrow$ disorder phase transition by varying the density and/or the noise, but is this also the case for a heterogeneous mixture?

2. If a phase transition is observed, what are the main differences? Is order promoted/suppressed?

3. Do spatial patterns arise and, if yes, how do they look like?

Three examples of heterogeneous biological systems. *Left:* two species of sheep forming a swirl. *Center:* schooling behaviour of a "binary mixture of fishes". *Right:* dolphins and their babies swimming together.

4. Under which circumstances are the two species bound together in their collective behaviour and under which other conditions do they separate in distinct phases?

The two most intuitive possibilities are illustrated in Fig. 5.

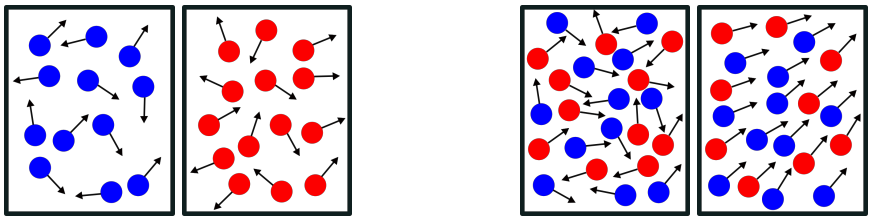

Figure 5: *Left:* Two ensembles of different (blue-red) self propelled particles moving in a disordered phase.They can for example differ by noise and/or density. *Right:* Two possible stationary states of the binary mixture formed by blue and red particles: homogeneous disorder or polar order.

Our system is composed of point-like particles that move in a well-defined direction on a plane, i.e. polar particles (see Fig. 1): both for intra-species collision and for inter-species ones a polar collision rule is retained. Note that this is a fundamental property of our system that affects all our following statements and results. Different collision rules would presumably lead to a different behaviour, already studied in the single species case [17, 20, 35].

After the definition of the Boltzmann approach to active matter and of our model, respectively in Sec. 2 and in Sec. 3, we derive the evolution equation of the two order parameters: one for each species.

To answer questions 1. and 2. we derive in Sec. 4 the phase diagram for the binary mixture with the two species being characterized by different density and noise. Linear stability reveals a net difference between the behaviour of two separated species and a binary mixture: we observe that by varying the noise of one of the two species, the other can undergo a non equilibrium phase transition. Order is enhanced

if one of the two species is already in an ordered state, otherwise the transition line is shifted to higher density values and disorder occupies most of the phase diagram. In this latter case we find that a density threshold has to be overcome to go from a disordered phase to an ordered one.

Motivated by the possibility of finding other analytical solutions of the equations of motion and thus other phases of our systems, we derive in Sec. 5 the hydrodynamic equations and show the non-existence of states where one species has zero average momentum and the other does not.

Finally, referring to question 3. and 4. we numerically solve in Sec.6 the Boltzmann equation for both species. We verify that spatial patterns (density waves) do arise close to the onset of order and that no demixing behaviour is present in our system.

2 The Boltzmann Equation

The whole kinetic theory relies on the assumption that a large number of particles ($N \approx \mathcal{N}_A$) can be described by means of a statistical theory based on simple assumptions, namely: the system is sufficiently diluted, all particles have the same characteristics, they collide with each other and diffuse due to the collisions between much smaller particles of the fluid in which they are suspended. As we will see, a great advantage of kinetic equations is that they describe mesoscopic particles at an intermediate scale between the microscopical and the hydrodynamical ones.

The usual approach starts from a Hamiltonian description of the system of N particles and with an equation for the one-particle density distribution function: the Boltzmann transport equation. Our derivation follows substantially the one given by D. Tong in [53] and is limited to the classical version devised by L. Boltzmann in 1872 [9]. It is again key to recall that a rigorous derivation of the Boltzmann equation is possible only for conservative systems: we will explicitly show in Sec. 2.3 that if the Boltzmann equation holds the system must evolve towards equilibrium. What we will indicate as the *kinetic Boltzmann equation* is more properly a heuristic ansatz verified a posteriori by simulations and experiments to be a correct description for this class of active systems.

2.1 Hamiltonian description and the BBGKY hierarchy

The Hamiltonian function for N identical particles is of the form

$$H = \sum_{i=1}^{N} \left[\frac{\mathbf{p}_i^2}{2m} + U(\mathbf{r}_i) \right] + \sum_{i<j} \mathcal{V}(\mathbf{r}_i - \mathbf{r}_j) \,. \tag{2.1}$$

On each particle acts an external force field $\mathbf{F} = -\nabla U$ and a force due to a two-body interaction potential that we have assumed to be dependent just on the mutual distance vector $\mathcal{V}(\mathbf{r}_i - \mathbf{r}_j)$. The Hamilton equations of motion for each particle read

$$\begin{aligned} \dot{\mathbf{r}}_i &= \frac{\partial H}{\partial \mathbf{p}_i} \\ \dot{\mathbf{p}}_i &= -\frac{\partial H}{\partial \mathbf{r}_i} \end{aligned} \tag{2.2}$$

but what we are mostly interested in is an evolution equation for the probability density function $f(\mathbf{r}, \mathbf{p}, t)$, where we have defined the N-dimensional vectors $\mathbf{r} = (\mathbf{r}_1, \cdots, \mathbf{r}_N)$ and $\mathbf{p} = (\mathbf{p}_1, \cdots, \mathbf{p}_N)$. The function f is defined in such a way that $f(\mathbf{r}, \mathbf{p}, t)\, d\mathbf{r} d\mathbf{p}$ is the probability that the system is in a state between $(\mathbf{r}, \mathbf{p})$ and

$(\mathbf{r}+d\mathbf{r},\mathbf{p}+d\mathbf{p})$ at time t. Normalization of f over the whole $6N$-dimensional phase space is also required

$$\int f(\mathbf{r},\mathbf{p},t)\,d\mathbf{r}\,d\mathbf{p}=1\,. \tag{2.3}$$

The derivative along the flow "$\frac{d}{dt}$" of the probability density is given by (using Einstein summation convention)

$$\frac{d}{dt}f=\frac{\partial f}{\partial t}+\frac{\partial f}{\partial \mathbf{r}_i}\cdot\dot{\mathbf{r}}_i+\frac{\partial f}{\partial \mathbf{p}_i}\cdot\dot{\mathbf{p}}_i \tag{2.4}$$

and as probability has to be conserved as the *Liouville theorem* states, then

$$\frac{d}{dt}f=0\quad\rightarrow\quad\frac{\partial f}{\partial t}=-\{f,H\}=\{H,f\}\,, \tag{2.5}$$

where we have substituted the Hamilton equations Eq. (2.2) into Eq. (2.4), we have used the definition of the *Poisson bracket* and its anticommutativity property

$$\{f,H\}=\frac{\partial f}{\partial \mathbf{r}_i}\cdot\frac{\partial H}{\partial \mathbf{p}_i}-\frac{\partial f}{\partial \mathbf{p}_i}\cdot\frac{\partial H}{\partial \mathbf{r}_i}\,, \tag{2.6}$$

$$\{f,H\}=-\{H,f\}\,. \tag{2.7}$$

This equation for all N particles is not really much of a help since the dependence is on all particle variables, so we concentrate on the *one-particle* distribution function defined by

$$f_1(\mathbf{r}_1,\mathbf{p}_1,t)=N\int d\mathbf{r}_2\cdots d\mathbf{r}_N\,d\mathbf{p}_2\cdots d\mathbf{p}_N\,f(\mathbf{r}_1,\mathbf{r}_2,\cdots\mathbf{r}_N,\mathbf{p}_1,\mathbf{p}_2\cdots\mathbf{p}_N) \tag{2.8}$$

and since all particles are identical we can take $\mathbf{r}_1=\mathbf{r}$, $\mathbf{p}_1=\mathbf{p}$. This function gives the probability that the system finds itself around the point $(\mathbf{r},\mathbf{p})$, where now the phase space is the single particle one (i.e. 6 dimensional). Eq. (2.3) together with Eq. (2.8) yields

$$\int d\mathbf{r}\,d\mathbf{p}\,f_1(\mathbf{r},\mathbf{p})=N\,. \tag{2.9}$$

The evolution in time of f_1 is obtained by relating it to the evolution equation for f Eq. (2.4)

$$\frac{\partial f_1}{\partial t}=N\int\prod_{i=2}^{N}d\mathbf{r}_i d\mathbf{p}_i\,\frac{\partial f}{\partial t}=N\int\prod_{i=2}^{N}d\mathbf{r}_i d\mathbf{p}_i\,\{H,f\}\,; \tag{2.10}$$

substituting the Hamiltonian in Eq. (2.1) and calculating the Poisson bracket, we can write (again in Einstein notation)

$$\frac{\partial f_1}{\partial t} = N \int \prod_{i=2}^{N} d\mathbf{r}_i d\mathbf{p}_i \left[-\frac{\mathbf{p}_j}{m} \cdot \frac{\partial f}{\partial \mathbf{r}_j} + \frac{\partial U(\mathbf{r}_j)}{\partial \mathbf{r}_j} \cdot \frac{\partial f}{\partial \mathbf{p}_j} + \sum_{l<m} \frac{\partial \mathcal{V}(\mathbf{r}_l - \mathbf{r}_m)}{\partial \mathbf{r}_j} \cdot \frac{\partial f}{\partial \mathbf{p}_j} \right] .$$

Now whenever $j = 2, \cdots, N$ we can integrate by parts and move the derivatives of f to the factors at their left. All of these vanish since they don't depend on the variable they are derived with respect to. The rest is a boundary term that vanishes because f itself has to be zero at $\pm\infty$. Finally, we are left just with $j = 1$ terms

$$\frac{\partial f_1}{\partial t} = N \int \prod_{i=2}^{N} d\mathbf{r}_i d\mathbf{p}_i \left[-\frac{\mathbf{p}_1}{m} \cdot \frac{\partial f}{\partial \mathbf{r}_1} + \frac{\partial U(\mathbf{r}_1)}{\partial \mathbf{r}_1} \cdot \frac{\partial f}{\partial \mathbf{p}_1} + \sum_{m=2}^{N} \frac{\partial \mathcal{V}(\mathbf{r}_1 - \mathbf{r}_m)}{\partial \mathbf{r}_1} \cdot \frac{\partial f}{\partial \mathbf{p}_1} \right] ,$$

so that recalling the definition Eq. (2.8)

$$\frac{\partial f_1}{\partial t} = \{H_1, f_1\} + N \int \prod_{i=2}^{N} d\mathbf{r}_i d\mathbf{p}_i \sum_{m=2}^{N} \frac{\partial \mathcal{V}(\mathbf{r} - \mathbf{r}_m)}{\partial \mathbf{r}} \cdot \frac{\partial f}{\partial \mathbf{p}} , \tag{2.11}$$

where we have defined the one-particle Hamiltonian

$$H_1 = \frac{|\mathbf{p}|^2}{2m} + U(\mathbf{r}) \tag{2.12}$$

and renamed $\mathbf{r}_1 = \mathbf{r}$, $\mathbf{p}_1 = \mathbf{p}$. At this point a natural question arises: how do we deal with the second term, since it seems that we cannot express it as a function of f_1 only? It is customary to rewrite Eq. (2.11) as

$$\frac{\partial f_1}{\partial t} = \{H_1, f_1\} + \left(\frac{\partial f_1}{\partial t} \right)_{coll} , \tag{2.13}$$

$\{H_1, f_1\}$ being the *streaming term* and $\left(\frac{\partial f_1}{\partial t}\right)_{coll}$ the *collisional term*. We can explicitly show that this second term is dependent on the *two-particle distribution function*

$$\begin{aligned} \left(\frac{\partial f_1}{\partial t} \right)_{coll} &= N(N-1) \int d\mathbf{r}_2 d\mathbf{p}_2 \frac{\partial \mathcal{V}(\mathbf{r} - \mathbf{r}_2)}{\partial \mathbf{r}} \\ &\cdot \frac{\partial}{\partial \mathbf{p}} \int \prod_{i=3}^{N} d\mathbf{r}_i d\mathbf{p}_i \, f(\mathbf{r}, \mathbf{r}_2, \cdots, \mathbf{p}, \mathbf{p}_2, \cdots, t) \\ &= \int d\mathbf{r}_2 d\mathbf{p}_2 \frac{\partial \mathcal{V}(\mathbf{r} - \mathbf{r}_2)}{\partial \mathbf{r}} \cdot \frac{\partial f_2}{\partial \mathbf{p}} , \end{aligned} \tag{2.14}$$

with the definition

$$f_2(\mathbf{r}_1, \mathbf{r}_2, \mathbf{p}_1, \mathbf{p}_2, t) = N(N-1) \int \prod_{i=3}^{N} d\mathbf{r}_i d\mathbf{p}_i \, f(\mathbf{r}_1, \mathbf{r}_2, \mathbf{r}_3, \cdots, \mathbf{p}_1, \mathbf{p}_2, \mathbf{p}_3, \cdots, t) \,. \tag{2.15}$$

It is easy to see that the hierarchy is not closed and the equation for f_2 has a contribution from f_3, the one for f_3 from f_4 and so on. In general the n-particle density function, defined by

$$\begin{aligned} &f_n(\mathbf{r}_1, \mathbf{r}_2, \cdots, \mathbf{r}_n, \mathbf{p}_1, \mathbf{p}_2, \cdots, \mathbf{p}_n, t) = \\ &\frac{N!}{(N-n)!} \int \prod_{i=n+1}^{N} d\mathbf{r}_i d\mathbf{p}_i \, f(\mathbf{r}_1, \mathbf{r}_2, \cdots, \mathbf{r}_n, \cdots, \mathbf{r}_N, \mathbf{p}_1, \mathbf{p}_2, \cdots, \mathbf{p}_n, \cdots, \mathbf{p}_N, t) \end{aligned} \tag{2.16}$$

obeys

$$\frac{\partial f_n}{\partial t} = \{H_n, f_n\} + \sum_{i=1}^{n} \int d\mathbf{r}_{n+1} d\mathbf{p}_{n+1} \frac{\partial \mathcal{V}(\mathbf{r}_i - \mathbf{r}_{n+1})}{\partial \mathbf{r}_i} \cdot \frac{\partial f_{n+1}}{\partial \mathbf{p}_i} \,, \tag{2.17}$$

which is known as the *BBGKY hierarchy*. The n-particle Hamiltonian including all interactions in between the n particles, reads

$$H_n = \sum_{i=1}^{n} \left[\frac{|\mathbf{p}_i|^2}{2m} + U(\mathbf{r}_i) \right] + \sum_{i<j\leq n} \mathcal{V}(\mathbf{r}_i - \mathbf{r}_j) \,. \tag{2.18}$$

Eq. (2.17) tells that the evolution of the n-particle density function has a *Liouville* streaming term and a collisional term that includes interaction with one of the particles outside the group of n. The form of this hierarchy of equations looks nevertheless ready to implement different kind of approximations, one of these is the Boltzmann equation.

2.2 Motivation and derivation

As explained in the preceding section, we must rely on precise assumptions in order to reduce the BBGKY hierarchy to a closed set of equations. The first and easiest possible is the one that Ludwig Boltzmann suggested in 1872: his main idea was to separate two different time scales that appear in the system. The first is the *mean-free time* τ between collisions and the second is the *collision time* τ_c i.e. the time during which a collision occurs. The first assumption is

$$\tau \gg \tau_c \tag{2.19}$$

so that the majority of the particles follow the hamiltonian flow for most of the time and occasional collisions occur within a much smaller time interval. We write down

the BBGKY hierarchy equations for f_1 and f_2:

one-particle distribution function

$$\left[\frac{\partial}{\partial t}+\frac{\mathbf{p}_1}{m}\cdot\frac{\partial}{\partial \mathbf{r}_1}\right] f_1 = \int d\mathbf{r}_2 d\mathbf{p}_2 \frac{\partial \mathcal{V}(\mathbf{r}-\mathbf{r}_2)}{\partial \mathbf{r}}\cdot\frac{\partial f_2}{\partial \mathbf{p}} \tag{2.20}$$

two-particle distribution function

$$\left[\frac{\partial}{\partial t}+\frac{\mathbf{p}_1}{m}\cdot\frac{\partial}{\partial \mathbf{r}_1}+\frac{\mathbf{p}_2}{m}\cdot\frac{\partial}{\partial \mathbf{r}_2}-\frac{\partial \mathcal{V}(\mathbf{r}_1-\mathbf{r}_2)}{\partial \mathbf{r}_1}\left(\frac{\partial}{\partial \mathbf{p}_1}-\frac{\partial}{\partial \mathbf{p}_2}\right)\right] f_2 = \int d\mathbf{r}_3 d\mathbf{p}_3 \left[\frac{\partial \mathcal{V}(\mathbf{r}_1-\mathbf{r}_3)}{\partial \mathbf{r}_1}\cdot\frac{\partial}{\partial \mathbf{p}_1}+\frac{\partial \mathcal{V}(\mathbf{r}_2-\mathbf{r}_3)}{\partial \mathbf{r}_2}\cdot\frac{\partial}{\partial \mathbf{p}_2}\right] f_3 \tag{2.21}$$

where the single particle potential U has been set to zero (in our particular case there will in fact be no external field acting on the particles). Each term in the equations scales as an inverse-time, so that we can distinguish between dominant terms and negligible ones. For example it is clear by looking at the assumption (2.19) that a term like

$$\frac{\partial \mathcal{V}}{\partial \mathbf{r}}\cdot\frac{\partial}{\partial \mathbf{p}} \sim \frac{1}{\tau_c} \tag{2.22}$$

will be dominant in the evolution of the density distributions. In Eq. (2.20) there is only one factor of this type, the one on the right side. Furthermore in Eq. (2.21) the term on the right is negligible: the integral is in fact non-zero only over the interaction range $d \ll \lambda$ (λ is the mean free path) of $\mathcal{V}$ due to Eq. (2.19). This means that since

$$\int d\mathbf{r}_3 d\mathbf{p}_3 \, f_3 \sim N f_2 \,,$$

the collision term on the right of Eq. (2.21) is reduced by a factor of Nd^3/V with respect to the one on the left. In our "dilute gas" assumption (see Eq. (2.19) or equivalently $d \ll \lambda$) we can then ignore it and obtain

$$\left[\frac{\partial}{\partial t}+\frac{\mathbf{p}_1}{m}\cdot\frac{\partial}{\partial \mathbf{r}_1}+\frac{\mathbf{p}_2}{m}\cdot\frac{\partial}{\partial \mathbf{r}_2}-\frac{\partial \mathcal{V}(\mathbf{r}_1-\mathbf{r}_2)}{\partial \mathbf{r}_1}\left(\frac{\partial}{\partial \mathbf{p}_1}-\frac{\partial}{\partial \mathbf{p}_2}\right)\right] f_2 \approx 0\,. \tag{2.23}$$

For the same reason the right side of Eq. (2.20) is reduced by Nd^3/V with respect to the left one, meaning that f_1 varies on the larger time scale τ. If we consider larger time scales than the one over which f_2 varies (τ_c), then we can assume that f_2 has

already reached equilibrium and set $\partial_t f_2 = 0$. This is justified by the fact that we want to look at the evolution of f_1 that varies much more slowly

$$\left[\frac{\mathbf{p}_1}{m}\cdot\frac{\partial}{\partial\mathbf{r}_1}+\frac{\mathbf{p}_2}{m}\cdot\frac{\partial}{\partial\mathbf{r}_2}-\frac{\partial\mathcal{V}(\mathbf{r}_1-\mathbf{r}_2)}{\partial\mathbf{r}_1}\left(\frac{\partial}{\partial\mathbf{p}_1}-\frac{\partial}{\partial\mathbf{p}_2}\right)\right]f_2=0\,. \tag{2.24}$$

Moreover, since the collision term in Eq. (2.24) affects only the relative position of the two particles, it is convenient to perform a linear canonical transformation to *relative* and *center of mass* coordinates, defined by

$$\begin{aligned}\mathbf{R}&=(\mathbf{r}_1+\mathbf{r}_2)/2\\ \mathbf{r}&=\mathbf{r}_1-\mathbf{r}_2\end{aligned}$$

for position, and for momentum by

$$\begin{aligned}\mathbf{P}&=\mathbf{p}_1+\mathbf{p}_2\\ \mathbf{p}&=(\mathbf{p}_1-\mathbf{p}_2)/2\end{aligned}$$

that clearly preserves the elementary Poisson brackets.
Eq. (2.24) transformed to the new coordinate system reads

$$\left[\frac{\mathbf{p}}{2m}\cdot\partial_{\mathbf{R}}+\frac{2\mathbf{p}}{m}\cdot\partial_{\mathbf{r}}-\frac{\partial\mathcal{V}(\mathbf{r})}{\partial\mathbf{r}}\cdot\partial_{\mathbf{p}}\right]f_2(\mathbf{r},\mathbf{R},\mathbf{p},\mathbf{P},t)=0$$

that, with the assumption $\partial_{\mathbf{R}} f_2 \ll \partial_{\mathbf{r}} f_2$, yields the useful form

$$\frac{\partial\mathcal{V}(\mathbf{r})}{\partial\mathbf{r}}\cdot\frac{\partial f_2}{\partial\mathbf{p}}=\frac{2\mathbf{p}}{m}\cdot\frac{\partial f_2}{\partial\mathbf{r}}\,. \tag{2.25}$$

We can finally rewrite the collision integral as

$$\begin{aligned}\left(\frac{\partial f_1}{\partial t}\right)_{coll}&=\int d\mathbf{r}_2\,d\mathbf{p}_2\,\frac{\partial\mathcal{V}(\mathbf{r}_1-\mathbf{r}_2)}{\partial\mathbf{r}_1}\cdot\frac{\partial f_2}{\partial\mathbf{p}_1}\\ &=\int d\mathbf{r}\,d\mathbf{p}_2\,\frac{\partial\mathcal{V}(\mathbf{r})}{\partial\mathbf{r}}\cdot\left[\frac{\partial}{\partial\mathbf{p}_1}-\frac{\partial}{\partial\mathbf{p}_2}\right]f_2\\ &=\frac{1}{m}\int_{|\mathbf{r}|<d}d\mathbf{r}\,d\mathbf{p}_2\,(\mathbf{p}_1-\mathbf{p}_2)\cdot\frac{\partial f_2}{\partial\mathbf{r}}\,,\end{aligned} \tag{2.26}$$

where we used integration by parts in the second line and Eq. (2.25) in the third one. In order to find an equation in which only f_1 appears, it is first convenient to use cylindrical coordinates defined such that the direction parallel to $|\mathbf{v}_1-\mathbf{v}_2|$ is

parametrized by x and the plane orthogonal to it by the radius-angle variables (ρ, θ). Because of the scalar product, in these new coordinates Eq. (2.26) becomes

$$\begin{aligned}\left(\frac{\partial f_1}{\partial t}\right)_{coll} &= \int d\mathbf{p}_2 |\mathbf{v}_1 - \mathbf{v}_2| \int \rho \, d\rho \int d\theta \int_{x_1}^{x_2} dx \frac{\partial f_2}{\partial x} \\ &= \int d\mathbf{p}_2 |\mathbf{v}_1 - \mathbf{v}_2| \int \rho \, d\rho \int d\theta \, [f_2(x_2) - f_2(x_1)] \, .\end{aligned}$$

At this point we consider the third fundamental assumption, that is usually called *molecular chaos*. What we require is that the two colliding particles are *uncorrelated* before and after the collision or in other words that we can write

before the collision

$$f_2(x_1) = f_1(\mathbf{r}, \mathbf{p}_1, t) f_1(\mathbf{r}, \mathbf{p}_2, t) \tag{2.27}$$

after the collision

$$f_2(x_2) = f_1(\mathbf{r}, \mathbf{p}_1', t) f_1(\mathbf{r}, \mathbf{p}_2', t) \, . \tag{2.28}$$

Note that both one-particle functions are evaluated at the same point in space since f_1 varies only on scales much bigger than the interaction range of the $\mathcal{V}$ potential. Using the definition of *differential cross-section* $d\sigma/d\Omega$

$$I \left| \frac{d\sigma}{d\Omega} \right| d\Omega = I \rho \, d\rho \, d\theta \tag{2.29}$$

where I is the beam *intensity* $\left([I] = \frac{\text{particles}}{\text{area} \cdot \text{time}} \right)$ and $d\Omega$ the solid angle, we can obtain the final form of Eq. (2.13)

$$\begin{aligned}\left[\frac{\partial}{\partial t} + \frac{\mathbf{p}_1}{m} \cdot \frac{\partial}{\partial \mathbf{r}_1} \right] f_1 = \int d\mathbf{p}_2 \, d\Omega \left| \frac{d\sigma}{d\Omega} \right| |\mathbf{v}_1 - \mathbf{v}_2| \\ \times \left[f_1(\mathbf{r}_1, \mathbf{p}_1', t) f_1(\mathbf{r}_1, \mathbf{p}_2', t) - f_1(\mathbf{r}_1, \mathbf{p}_1, t) f_1(\mathbf{r}_1, \mathbf{p}_2, t) \right] \, .\end{aligned} \tag{2.30}$$

The Boltzmann equation can also be derived using a more euristic and intuitive procedure: the rate at which the scattering process occurs, namely the probability that, per unit time, two particles with momenta $\mathbf{p}$ and $\mathbf{p}_2$ emerge from the collision at position r with momenta $\mathbf{p}_1'$ and $\mathbf{p}_2'$, will be proportional to the two particle density function

$$\Delta = \omega(\mathbf{p}_1', \mathbf{p}_2'; \mathbf{p}, \mathbf{p}_2) \, f_2(\mathbf{r}, \mathbf{r}, \mathbf{p}, \mathbf{p}_2) \, d\mathbf{p}_2 \, d\mathbf{p}_1' \, d\mathbf{p}_2' \, ; \tag{2.31}$$

we also need to consider that collisions not only deflect particles into a state with momentum $\mathbf{p}$, but they can deflect them out of such a state into one with a different

momentum $\mathbf{p}'$. There will then be a *gain* term and a *loss* term in the collision integral

$$\left(\frac{\partial f_1}{\partial t}\right)_{coll} = \int d\mathbf{p}_2 d\mathbf{p}_2' d\mathbf{p}_1' [\omega(\mathbf{p}, \mathbf{p}_2; \mathbf{p}_1', \mathbf{p}_2') f_2(\mathbf{r}, \mathbf{r}, \mathbf{p}_1', \mathbf{p}_2') - \omega(\mathbf{p}_1', \mathbf{p}_2'; \mathbf{p}, \mathbf{p}_2) f_2(\mathbf{r}, \mathbf{r}, \mathbf{p}, \mathbf{p}_2)] \,. \tag{2.32}$$

Invariance of the rate under time reversal and parity $(\mathbf{r}, \mathbf{p}) \to (-\mathbf{r}, -\mathbf{p})$ transformations implies that the scattering rate must be invariant under exchange of incoming and outgoing momenta

$$\omega(\mathbf{p}, \mathbf{p}_2; \mathbf{p}_1', \mathbf{p}_2') = \omega(\mathbf{p}_1', \mathbf{p}_2'; \mathbf{p}, \mathbf{p}_2) \,; \tag{2.33}$$

furthermore the *molecular chaos* assumption

$$f_2(\mathbf{r}, \mathbf{r}, \mathbf{p}, \mathbf{p}_2) = f_1(\mathbf{r}, \mathbf{p}) f_1(\mathbf{r}, \mathbf{p}_2) \tag{2.34}$$

allows us to rewrite Eq. (2.32) as

$$\left(\frac{\partial f_1}{\partial t}\right)_{coll} = \int d\mathbf{p}_2 d\mathbf{p}_2' d\mathbf{p}_1' \omega(\mathbf{p}, \mathbf{p}_2; \mathbf{p}_1', \mathbf{p}_2') \left[f_1(\mathbf{r}, \mathbf{p}_1') f_1(\mathbf{r}, \mathbf{p}_2') - f_1(\mathbf{r}, \mathbf{p}) f_1(\mathbf{r}, \mathbf{p}_2)\right] .$$

This is exactly equal to Eq. (2.30) if we set $\omega(\mathbf{p}, \mathbf{p}_2; \mathbf{p}_1', \mathbf{p}_2') = |\mathbf{v} - \mathbf{v}_2| \left|\frac{d\sigma}{d\Omega}\right| d\Omega$. This derivation has the advantage of being much more intuitive and less intricate than the formal one; nevertheless the latter has a direct connection with the Hamiltonian description and thus is mathematically more justified.
Even if it already relies on more than one assumption, the Boltzmann equation is a nontrivial integro-differential equation that apart from some simple cases is not easily solvable. Nonetheless it is one of the most successful and used equations in statistical physics: it correctly predicts the thermodynamics of a Maxwell gas, a slightly modified "semiclassical" version of it is able to describe transport of electrons in a metal and, last but not least, it provides a connection between the microscopic (time reversal symmetric) picture and the macroscopic one (where a "time arrow" is present). This bridge between macroscopic and microscopic world becomes evident when in the next section we prove that all systems that obey the Boltzmann equation, relax to equilibrium in an irreversible fashion. Note that this also means that if the system is a non-equilibrium one, then the Boltzmann equation doesn't hold: this is why our ansatz to employ a slightly modified version of this equation to describe our non equilibrium system is a heuristic one.

2.3 The $\mathcal{H}$-theorem

The fundamental quantity introduced by Boltzmann is the $\mathcal{H}$-function, defined by

$$\mathcal{H}(t) = \int d\mathbf{r}\, d\mathbf{p}\, f_1(\mathbf{r}, \mathbf{p}, t) \log f_1(\mathbf{r}, \mathbf{p}, t) \,, \tag{2.35}$$

which is related to the entropy $S = -k_B f_1 \log f_1$ via $S = -k_B \mathcal{H}$. The $\mathcal{H}$-theorem proves that the $\mathcal{H}$-function is non-increasing in time, i.e. $\frac{d}{dt}\mathcal{H}(t) \leq 0$. We first take the time derivative of Eq. (2.35)

$$\frac{d\mathcal{H}}{dt} = \int d\mathbf{r}\, d\mathbf{p}\, (\log f_1 + 1)\frac{\partial f_1}{\partial t} = \int d\mathbf{r}\, d\mathbf{p}\, \log f_1 \frac{\partial f_1}{\partial t}$$

where we have dropped the $+1$ term since $\int d\mathbf{r}\, d\mathbf{p}\, \partial_t f_1 = \partial_t \int d\mathbf{r}\, d\mathbf{p}\, f_1 = 0$. We then substitute the Boltzmann equation(2.13)

$$\frac{d\mathcal{H}}{dt} = \int d\mathbf{r}\, d\mathbf{p}\, \log f_1 \left[\frac{\partial U}{\partial \mathbf{r}} \cdot \frac{\partial f_1}{\partial \mathbf{p}} - \frac{\mathbf{p}}{m} \cdot \frac{\partial f_1}{\partial \mathbf{r}} + \left(\frac{\partial f_1}{\partial t}\right)_{coll}\right];$$

the first two terms vanish just integrating by parts twice

$$\int d\mathbf{r}d\mathbf{p} \log f_1 \frac{\partial U}{\partial \mathbf{r}} \cdot \frac{\partial f_1}{\partial \mathbf{p}} = -\int\int d\mathbf{r}d\mathbf{p} \frac{\partial U}{\partial \mathbf{r}} \cdot \frac{\partial \log f_1}{\partial \mathbf{p}} f_1 = \int d\mathbf{r}d\mathbf{p} \nabla_p \cdot \left(\frac{\partial U}{\partial \mathbf{r}}\right) f_1 = 0$$

where we have dropped all contour terms that vanish at infinity because of the normalization condition of f_1.
In the end what governs the evolution of the $\mathcal{H}$-function is only the collision term

$$\begin{aligned}\frac{d\mathcal{H}}{dt} &= \int d\mathbf{r}d\mathbf{p} \log f_1 \left(\frac{\partial f_1}{\partial t}\right)_{coll} \\ &= \int d\mathbf{r}d\mathbf{p}_1 d\mathbf{p}_2 d\mathbf{p}_2' d\mathbf{p}_1' \omega(\mathbf{p}_1, \mathbf{p}_2; \mathbf{p}_1', \mathbf{p}_2') \log f_1(\mathbf{p}_1) \left[f_1(\mathbf{p}_1')f_1(\mathbf{p}_2') - f_1(\mathbf{p}_1)f_1(\mathbf{p}_2)\right].\end{aligned} \tag{2.36}$$

We can make Eq. (2.36) more symmetric in the indices $1 \Leftrightarrow 2$ just by switching the dummy integration variable $\mathbf{p}_2 \Leftrightarrow \mathbf{p}_2$

$$\frac{d\mathcal{H}}{dt} = \int d\mathbf{r}d\mathbf{p}_1 d\mathbf{p}_2 d\mathbf{p}_2' d\mathbf{p}_1' \omega(\mathbf{p}_1, \mathbf{p}_2; \mathbf{p}_1', \mathbf{p}_2') \log f_1(\mathbf{p}_2) \left[f_1(\mathbf{p}_1')f_1(\mathbf{p}_2') - f_1(\mathbf{p}_1)f_1(\mathbf{p}_2)\right] \tag{2.37}$$

and then sum the two to obtain

$$\begin{aligned}\frac{d\mathcal{H}}{dt} = \frac{1}{2}\int d\mathbf{r}d\mathbf{p}_1 d\mathbf{p}_2 d\mathbf{p}_2' d\mathbf{p}_1' \, \omega(\mathbf{p}_1, \mathbf{p}_2; \mathbf{p}_1', \mathbf{p}_2') \log(f_1(\mathbf{p}_2)f_1(\mathbf{p}_1)) \\ \times \left[f_1(\mathbf{p}_1')f_1(\mathbf{p}_2') - f_1(\mathbf{p}_1)f_1(\mathbf{p}_2)\right].\end{aligned} \tag{2.38}$$

If we now swap the primed variables and the non-primed ones $\mathbf{p}' \Leftrightarrow \mathbf{p}$, we are just exchanging incoming and outgoing momenta so that the scattering rate remains the same as assured by the property Eq. (2.33)

$$\begin{aligned}\frac{d\mathcal{H}}{dt} = -\frac{1}{2}\int d\mathbf{r}d\mathbf{p}_1 d\mathbf{p}_2 d\mathbf{p}_2' d\mathbf{p}_1' \, \omega(\mathbf{p}_1, \mathbf{p}_2; \mathbf{p}_1', \mathbf{p}_2') \log(f_1(\mathbf{p}_2')f_1(\mathbf{p}_1')) \\ \times \left[f_1(\mathbf{p}_1')f_1(\mathbf{p}_2') - f_1(\mathbf{p}_1)f_1(\mathbf{p}_2)\right];\end{aligned}$$

finally we sum the last two equations

$$\frac{d\mathcal{H}}{dt} = -\frac{1}{2}\int d\mathbf{r}d\mathbf{p}_1 d\mathbf{p}_2 d\mathbf{p}_2' d\mathbf{p}_1'\, \omega(\mathbf{p}_1,\mathbf{p}_2;\mathbf{p}_1',\mathbf{p}_2') \\ \times \log(f_1(\mathbf{p}_2')f_1(\mathbf{p}_1') - f_1(\mathbf{p}_2)f_1(\mathbf{p}_1))\left[f_1(\mathbf{p}_1')f_1(\mathbf{p}_2') - f_1(\mathbf{p}_1)f_1(\mathbf{p}_2)\right] .$$

Since the function $(\log x - \log y)(x-y)$ is always non-negative and so is the scattering rate, we have proved that

$$\frac{d\mathcal{H}}{dt} \leq 0\,. \tag{2.39}$$

As already noted, this is equivalent to state that $\partial_t S \geq 0$; this means that we have introduced a time arrow in our equations, such that now we are able to distinguish between a system that is evolving further in time and one that is evolving backwards. But where exactly did we introduce irreversibility in our derivation of the Boltzmann equation, since we started from an Hamiltonian theory that is fully invariant under time reversal symmetry? The answer is to be found in one of our assumptions, in particular in the *molecular chaos* assumption Eq. (2.34): there we required the two particles to be uncorrelated *before the collision* and so we took $f_2 \sim f_1 f_1$.

To summarize, we list all assumptions that led to the Boltzmann equation in the form

$$\left[\frac{\partial}{\partial t} + \frac{\mathbf{p}}{m}\cdot\frac{\partial}{\partial \mathbf{r}} - \frac{\partial U}{\partial \mathbf{r}}\cdot\frac{\partial}{\partial \mathbf{p}}\right] f_1 = \int d\mathbf{p}_2 d\mathbf{p}_2' d\mathbf{p}_1' \omega(\mathbf{p},\mathbf{p}_2;\mathbf{p}_1',\mathbf{p}_2') \\ \times \left[f_1(\mathbf{r},\mathbf{p}_1')f_1(\mathbf{r},\mathbf{p}_2') - f_1(\mathbf{r},\mathbf{p})f_1(\mathbf{r},\mathbf{p}_2)\right] \tag{2.40}$$

- the system is sufficiently dilute so that only binary collisions occur (time scale separation);

- particles move with constant velocity between collisions and undergo classical scattering events;

- molecular chaos: $f_2(\mathbf{r},\mathbf{r},\mathbf{p},\mathbf{p}_2) = f_1(\mathbf{r},\mathbf{p})f_1(\mathbf{r},\mathbf{p}_2)$.

3 Model Definition

The purpose of this section is first to define the model that is customarily used to describe two-dimensional dry active systems via the Boltzmann equation [6, 7, 37] and to extend it to binary mixtures of particles. We will first extensively describe how the model is constructed for a *single species* of particles and then in Sect. 3.5 we will naturally extend it to a system of two interacting species. The first simplifying assumption of this model (and of many others) is to look at particles on a plane. We will see that making use of Fourier series and the correspondence between two dimensional vectors and complex numbers allows for a great simplification of the equations.

3.1 The kinetic Boltzmann equation for dry active systems

While constructing the model we need to take into account the fact that we are describing particles that, if collisions and diffusion are removed, are ballistic ones, meaning that they move on a straight line with constant speed. Fixing the velocity means breaking the Galilean invariance of the equations of motion and non conservation of momentum during collisions. Given the spatial "resolution" of the Boltzmann equation (remember that the interaction range is considered to be much smaller than the typical distance over which the distribution function varies appreciably) we will model our collisions using aligning "collision rules" that almost completely forget about microscopic details. The one particle density distribution $f_1(\mathbf{r}, \theta, t)$ is a function of the two spatial variables $\mathbf{r} = (x, y)$, an angular one and of course of time. The particles of our systems don't move in vacuum, but on a substrate that is able to absorb momentum (as already anticipated in the introduction these systems where momentum is *not* conserved are called "dry", while a system where momentum is conserved is called "wet" [29]); the collisions of our suspended particles with the much smaller particles of the substrate introduce random noise called "external". Furthermore our particle can undergo random fluctuations because of some source of internal noise. We introduce random noise onto the angular variable to take these two effects into account. We thus consider the so called self-diffusion events where the angle θ_i of the velocity $\mathbf{v}_i$ of a particle changes with constant rate λ during each time step

$$\theta \xrightarrow{\lambda} \theta' = \theta + \eta \,,$$

where η is a random variable distributed according to a Gaussian distribution $P_d(\eta)$ with variance σ_d^2.

Since the momentum dependence has reduced to an angular dependence, we also need to modify the collision integral: the gain term is due to particles that

are scattered into the θ direction, whereas the loss term has contributions from all particles that, from the θ direction are scattered into any other. Furthermore we will introduce a stochastic noise on top of the post-collisional angle to simulate our uncertainty on the outcome of a collision. The angles of two particles are then modified in a collision

$$\theta_1 \to \Psi(\theta_1, \theta_2) + \eta_1 \,, \quad \theta_2 \to \Psi(\theta_1, \theta_2) + \eta_2$$

η_1 and η_2 being two independent Gaussian variables with variance σ_c^2, whereas $\Psi(\theta_1, \theta_2)$ is the outgoing angle according to some pre-defined *interaction rule*. The form and periodicity of Ψ depend on the type of collision we are looking at: polar, antipolar or nematic (for a precise definition of all collision rules see App. A). One important feature of Ψ is that it only depends on the difference of the two angular variables, due to the isotropy of the system. If we rotate both angles by the same amount ϕ

$$\Psi(\theta_1 + \phi, \theta_2 + \phi) = \Psi(\theta_1, \theta_2) + \phi + k\pi, \quad k \in \mathbb{Z} \tag{3.1}$$

so that by choosing $\phi = -\theta_1$ and $\Delta = \theta_2 - \theta_1$

$$\Psi(\theta_1, \theta_2) = \theta_1 + \Psi(0, \Delta) + k\pi. \tag{3.2}$$

From now on we will choose $\Psi(0, \Delta) = \Psi(\Delta) = \Delta/2$ so that the outgoing angle is defined to be the average of the two incoming ones

$$\psi(\theta_1, \theta_2) = \theta_1 + \Delta/2 = (\theta_1 + \theta_2)/2 \,. \tag{3.3}$$

Another interesting property of Ψ that holds in the case of *non-chiral particles* is the invariance for exchange of the two variables ($\theta_1 \Leftrightarrow \theta_2$)

$$\Psi(\theta_1, \theta_2) = \Psi(\theta_2, \theta_1) \quad or \quad \Psi(-\Delta) = \Psi(\Delta). \tag{3.4}$$

For a *polar* or an *antipolar* collision rule Ψ is 2π periodic in both angles θ_1 and θ_2 (modulo 2π) or in the unique variable Δ, whereas for a *nematic* collision, periodicity is π. We will from now on consider *polar* collisions, unless explicitly stated otherwise.

It's worth noting that effectively, what we are describing are particles performing a persistent random walk (a random walk where the walker has a definite probability of continuing in the same direction as the previous step) and abruptly colliding with each other.

Taking all these facts into account, we can rewrite the Boltzmann equation in the following generalized way

$$\left[\frac{\partial}{\partial t} + v_0 \mathbf{e}_\theta \cdot \frac{\partial}{\partial \mathbf{r}}\right] f(\mathbf{r}, \theta, t) = I_d[f] + I_c[f] \,, \tag{3.5}$$

where I_d accounts for self-diffusion events and I_c for binary collisions. These two integrals are of the form

$$I_d[f] = -\lambda f(\theta) + \lambda \int_{-\pi}^{\pi} d\theta' \int_{-\infty}^{\infty} d\eta P_0(\eta) \delta_{2\pi}(\theta' + \eta - \theta) f(\theta') \,; \tag{3.6}$$

$$\begin{aligned} I_c[f] = -f(\theta) \int_{-\pi}^{\pi} d\theta' R(\theta', \theta) f(\theta') + \int_{-\pi}^{\pi} d\theta_1 d\theta_2 R(\theta_1, \theta_2) f(\theta_1) f(\theta_2) \\ \times \int_{-\infty}^{\infty} d\eta P(\eta) \delta_{2\pi}(\Psi(\theta_1, \theta_2) + \eta - \theta) \,. \end{aligned} \tag{3.7}$$

where we used the short notation $\delta_{2\pi}(\theta)$ instead of $\sum_{m\in\mathbb{Z}} \delta(\theta + 2m\pi)$ to indicate the dirac delta modulo 2π. In the collision term we have inserted the so called *collision kernel* R. In metric models, where the interaction takes place if the distance between particles is smaller than a certain range, collisions can be modelled as scattering processes and the collision kernel or *cross section* can be expressed as we explain in the next section.

3.2 Cross section

The rate of collision between two particles with momentum in direction θ_1 and θ_2 is given by $R(\theta_1, \theta_2)$. Its meaning is straightforward: the gain in particles (or in the function f) at point $(\mathbf{r}, \theta, t)$ is given by the fraction of particles that enter the collision range with momentum in direction θ' i.e. $f(\mathbf{r}, \theta', t)$, times the probability of being scattered into direction θ i.e. $R(\theta, \theta')f(\theta)$ summed over all possible initial directions θ'. The analytic expression of R can in general depend both on the different shape of the incoming particles and on their direction: here due to isotropy reasons $R = R(\Delta)$ and our collisions will be between rod-shaped particles, defined via the *aspect ratio* ξ i.e. the ratio between the particle's length and its diameter (more precisely the diameter of the cylinder, if we think of a rod as being composed by a cylindrical shape with rounded ends).

$$\xi = l/d \tag{3.8}$$

and for *spherical* particles (the only case we considered so far) $\xi = 1$.

As already pointed out in the derivation of the equilibrium Boltzmann equation, the cross section can be thought of as being the area of collision between the two particles per infinitesimal time step dt. It is easier to figure out what the collisional area is, if we go to the rest frame of particle 1. We can convince ourselves that in order to collide with particle 1, particle 2 has to be inside the area A which has three

separate contributions, namely S_1, S_2, S_3 as indicated in Fig. 6

$$S_2 = l v_{rel} |\sin(\Delta)| dt$$
$$S_1 + S_3 = d\, v_{rel} dt \int_{-\Delta}^{\pi-\Delta} d\phi \sin(\phi + \Delta) = 2 d v_{rel} dt \tag{3.9}$$

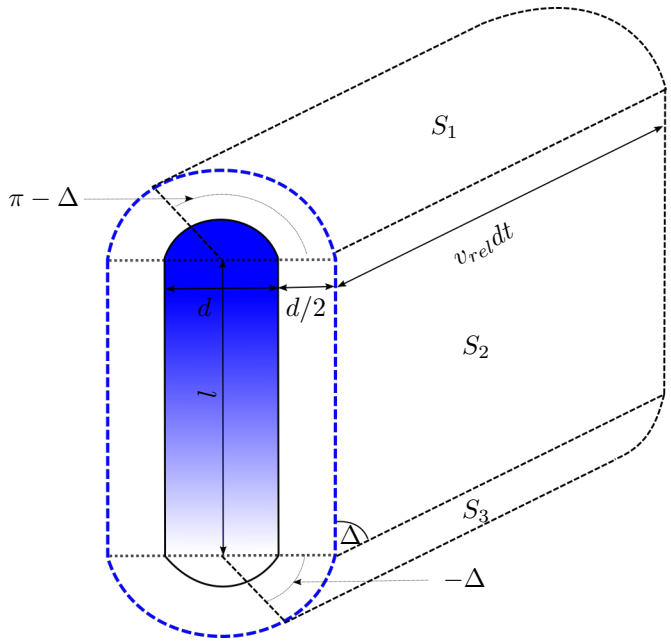

Figure 6: Sketch of the cross sectional area in the rest frame of particle 1.

Going back to the rest frame of the laboratory we have $\Delta = \theta_2 - \theta_1$ and $v_{rel} = v_0 |\mathbf{e}_{\theta_2} - \mathbf{e}_{\theta_2}|$, thus the cross section reads

$$R(\Delta) = v_0 |\mathbf{e}_{\theta_2} - \mathbf{e}_{\theta_1}| (l |\sin(\Delta)| + 2d) \tag{3.10}$$

that can be rewritten using the definitions $\mathbf{e}_{\theta_2} = (\cos\theta_2, \sin\theta_2)$, $\mathbf{e}_{\theta_1} = (\cos\theta_1, \sin\theta_1)$, $\xi = (l + d)/d$ and the trigonometric relation $\sin^2(\Delta/2) = (1 - \cos\Delta)/2$

$$R(\Delta) = 4 v_0 d |\sin(\Delta/2)| \left(1 + \frac{\xi - 1}{2} |\sin\Delta|\right) . \tag{3.11}$$

Note that if we are dealing with spherical particles $\xi = 1$ so that $R(\Delta) = 4 v_0 d |\sin(\Delta/2)|$.

3.3 Expansion in Fourier series

Since $f(\mathbf{r}, \theta, t)$ is a periodic function of the angular variable θ, it is more convenient to study the evolution of its Fourier modes defined by

$$\hat{f}_k(\mathbf{r}, t) = \int_{-\pi}^{+\pi} d\theta \, e^{ik\theta} f(\mathbf{r}, \theta, t) \qquad \theta \in (-\pi, \pi],\, k \in \mathbb{Z} \tag{3.12}$$

instead of looking at the evolution of the real function $f(\mathbf{r}, \theta, t)$. Particularly important are the first three modes: the zero moment is nothing but the particle density as can be immediately seen from its definition

$$\hat{f}_0(\mathbf{r}, t) = \int d\theta f(\mathbf{r}, \theta, t) = \rho(\mathbf{r}, t)\,; \tag{3.13}$$

the *polar order field* $\mathbf{P}$ is instead defined by

$$\mathbf{P} = \begin{pmatrix} \langle \cos\theta \rangle \\ \langle \sin\theta \rangle \end{pmatrix} = \int d\theta f(\mathbf{r}, \theta, t)\, \mathbf{e}_\theta\,, \tag{3.14}$$

$\mathbf{e}_\theta = (\cos(\theta), \sin(\theta))^T$ being the "polar" unit vector. We can immediately relate the first moment of the probability density distribution

$$\hat{f}_1 = \int d\theta \, e^{i\theta} f(\theta) \tag{3.15}$$

to the polar order field via

$$\rho\mathbf{P} = \begin{pmatrix} \mathrm{Re}\hat{f}_1 \\ \mathrm{Im}\hat{f}_1 \end{pmatrix} \tag{3.16}$$

or equivalently to the *momentum field* via

$$\mathbf{p}(\mathbf{r}, t) = \rho(\mathbf{r}, t)\mathbf{P}(\mathbf{r}, t)\,. \tag{3.17}$$

Finally, the second mode of the Fourier expansion

$$\hat{f}_2 = \int d\theta \, e^{2i\theta} f(\theta) \tag{3.18}$$

corresponds to the *nematic tensor field* since the factor $e^{i2\theta}$ is π periodic. Nematic order is particularly important in the theory of liquid crystals [16]: adapted to our "probabilistic" approach, the nematic tensorial field is defined as

$$\rho\mathbf{Q} = \frac{1}{2} \begin{pmatrix} \langle \cos(2\theta) \rangle & \langle \sin(2\theta) \rangle \\ \langle \sin(2\theta) \rangle & -\langle \cos(2\theta) \rangle \end{pmatrix}. \tag{3.19}$$

It is straightforward to relate the definition Eq. (3.19) to the second Fourier mode

$$\rho\mathbf{Q} = \frac{1}{2}\begin{pmatrix} \mathrm{Re}\hat{f}_2 & \mathrm{Im}\hat{f}_2 \\ \mathrm{Im}\hat{f}_2 & -\mathrm{Re}\hat{f}_2 \end{pmatrix} . \tag{3.20}$$

By inverting Eq. (3.12), the probability density can be expanded in Fourier series

$$f(\mathbf{r},\theta,t) = \frac{1}{2\pi}\sum_{k=0}^{\infty} \hat{f}_k(\mathbf{r},t)e^{-ik\theta} , \tag{3.21}$$

where following properties hold for all modes:

$$\int d\theta e^{ik\theta} = 2\pi\delta_{k,0} \tag{3.22}$$

and

$$\sum_{k=0}^{\infty} e^{-ik\theta} = 2\pi\delta(\theta) , \tag{3.23}$$

that assure consistency with Eq. (3.21) and Eq. (3.12).

We would like to stress that expressing the density function via its Fourier modes is a fundamental point of the whole analysis, since it allows many simplifications (especially in the diffusion and in the collision integrals) and moves the attention to the polar order vector field, which is the one that ultimately determines whether a polar system like ours is ordered or not (it is in practice the order parameter for the system). From now on we will always work in Fourier space, except when we will describe the numerical solver for the Boltzmann equation (SNAKE). This algorithm solves the Boltzmann equation in *real* space, via a discretization of time and space.

We will now apply these definitions to the Eq. (3.5), transforming it in an evolution equation for each Fourier mode:

1.
$$\int d\theta e^{ik\theta}\partial_t f = \partial_t \int d\theta e^{ik\theta} f = \partial_t \hat{f}_k ; \tag{3.24}$$

2.
$$\begin{aligned} &\int d\theta e^{ik\theta} v_0 \mathbf{e}_\theta \cdot \partial_{\mathbf{r}} f = v_0 \partial_{\mathbf{r}} \cdot \int d\theta e^{ik\theta} \begin{pmatrix} \cos\theta \\ \sin\theta \end{pmatrix} f(\mathbf{r},\theta,t) \\ &= v_0\partial_x \int d\theta e^{ik\theta}\cos\theta f + v_0\partial_y \int d\theta e^{ik\theta}\sin\theta\, f(\mathbf{r},\theta,t) \\ &= \frac{1}{2}v_0\partial_x \int d\theta e^{ik\theta}(e^{i\theta}+e^{-i\theta})f - \frac{i}{2}v_0\partial_y \int d\theta (e^{i\theta}-e^{-i\theta})f \\ &= \frac{1}{2}v_0(\partial_x - i\partial_y)\hat{f}_{k+1} + \frac{1}{2}v_0(\partial_x + i\partial_y)\hat{f}_{k-1} ; \end{aligned} \tag{3.25}$$

3.

$$\begin{aligned}\int d\theta e^{ik\theta} I_d[f] &= -\lambda \int d\theta e^{ik\theta} f + \lambda \int_{-\pi}^{\pi} d\theta' \int_{-\infty}^{\infty} d\eta P_0(\eta) \\ &\times \int d\theta e^{ik\theta} \delta_{2\pi}(\theta' + \eta - \theta) f \\ &= -\lambda \hat{f}_k + \lambda \int_{-\pi}^{\pi} d\theta' \int_{-\infty}^{\infty} d\eta P_0(\eta) \int d\theta e^{ik\theta} \\ &\times \delta_{2\pi}(\theta' + \eta - \theta) f(\theta') \\ &= -\lambda \hat{f}_k + \lambda \int_{-\pi}^{\pi} d\theta' \int_{-\infty}^{\infty} d\eta P_0(\eta) e^{ik(\theta'+\eta)} f(\theta') \\ &= -\lambda \hat{f}_k + \lambda \int_{-\infty}^{\infty} d\eta P_0(\eta) e^{ik\eta} \int_{-\pi}^{\pi} d\theta' f(\theta') \\ &= \lambda (P_{0,k} - 1) \hat{f}_k \,,\end{aligned} \tag{3.26}$$

where

$$P_{0,k} = \int_{-\infty}^{\infty} d\eta P_0(\eta) e^{ik\eta} = e^{-k^2 \sigma_d^2/2} \tag{3.27}$$

is the Fourier transform of the Gaussian distribution $P_0(\eta)$;

4.

$$\begin{aligned}\int d\theta e^{ik\theta} I_c[f] &= \int d\theta e^{ik\theta} \big[- f(\theta) \int_{-\pi}^{\pi} d\theta' R(\theta', \theta) f(\theta') \\ &+ \int_{-\pi}^{\pi} d\theta_1 d\theta_2 R(\theta_1, \theta_2) f(\theta_1) f(\theta_2) \int_{-\infty}^{\infty} d\eta P(\eta) \\ &\times \delta_{2\pi}(\Psi(\theta_1, \theta_2) + \eta - \theta) \big] \,.\end{aligned} \tag{3.28}$$

We calculate Eq. (3.28) in two different steps: first the loss term (L)

$$\begin{aligned} I^L_{c,k} &= - \int d\theta e^{ik\theta} f(\theta) \int_{-\pi}^{\pi} d\theta' R(\theta' - \theta) f(\theta') \\ &= - \int d\theta e^{ik\theta} \frac{1}{2\pi} \sum_p \hat{f}_p e^{-ip\theta} \int_{-\pi}^{\pi} d\theta' R(\theta' - \theta) \frac{1}{2\pi} \sum_q \hat{f}_q e^{-iq\theta'} \\ &= - \frac{1}{(2\pi)^2} \int d\theta e^{ik\theta} \sum_p \hat{f}_p e^{-ip\theta} \int_{-\pi}^{\pi} d\theta' \sum_q \hat{f}_q e^{-iq\theta'} R(\theta' - \theta) \,, \end{aligned}$$

and use the substitution $\theta' - \theta = \Delta$, paying attention to the fact that $\Delta \in (-\pi - \theta, \pi - \theta] = (-\pi, \pi]$ because we are dealing with angular variables on a circle.

$$
\begin{aligned}
&- \frac{1}{(2\pi)^2} \sum_{p,q} \hat{f}_p \hat{f}_q \int d\theta e^{ik\theta} e^{-ip\theta} e^{-iq\theta} \int_{-\pi}^{\pi} d\Delta e^{-iq\Delta} R(\Delta) \\
&= -\frac{1}{(2\pi)^2} \sum_{p,q} \hat{f}_p \hat{f}_q \underbrace{\int d\theta e^{i(k-p-q)\theta}}_{=2\pi\delta_{k-p-q,0}} \int_{-\pi}^{\pi} d\Delta e^{-iq\Delta} R(\Delta) \\
&= -\frac{1}{2\pi} \sum_{q} \hat{f}_{k-q} \hat{f}_q \int_{-\pi}^{\pi} d\Delta e^{-iq\Delta} R(\Delta) \,,
\end{aligned}
$$

and $\int_{-\pi}^{\pi} d\Delta e^{-iq\Delta} R(\Delta) = \int_{-\pi}^{\pi} d\Delta \cos(q\Delta) R(\Delta)$ because of the symmetry of the integration range and the odd parity of the integrand function.

The *loss* term is then

$$
I^L_{c,k} = -\frac{1}{2\pi} \sum_{q} \hat{f}_{k-q} \hat{f}_q \int_{-\pi}^{\pi} d\Delta \cos(q\Delta) R(\Delta) \,. \tag{3.29}
$$

The *gain* term (G) involves also the collision rule and since its Fourier transform involves some lines of calculations, we will give here the final result and postpone the complete calculation to App. A. Furthermore, as already remarked, we will consider only *polar* collisions where both R and Ψ are 2π periodic. [1]

$$
I^G_{c,k} = \frac{1}{2\pi} \sum_{q} \hat{f}_q \hat{f}_{k-q} P_k \int d\Delta R(\Delta) \cos((q - k/2)\Delta) \,. \tag{3.30}
$$

By summing the two contributions given by Eq. (3.29) and Eq. (3.30) we can express the result in the following form

$$
I_{c,k} = I^L_{c,k} + I^G_{c,k} = \sum_{q=-\infty}^{\infty} I_{q,k} \hat{f}_q \hat{f}_{k-q} \,, \tag{3.31}
$$

with

$$
I_{q,k} = \int_{-\pi}^{\pi} \frac{d\Delta}{2\pi} R(\Delta) \left[P_k \cos((q - k/2)\Delta) - \cos(q\Delta) \right] \tag{3.32}
$$

and

$$
P_k = \int_{-\infty}^{\infty} d\eta P(\eta) e^{ik\eta} = e^{-k^2\sigma^2/2} \,. \tag{3.33}
$$

[1] In the App. A a short derivation is given in the case of *antipolar* and *nematic* collision rules.

Collecting all transformed terms, we can write down the evolution equation for each Fourier mode $\hat{f}_k$

$$\partial_t \hat{f}_k + \frac{1}{2} v_0 (\partial_x - i\partial_y)\hat{f}_{k+1} + \frac{1}{2} v_0 (\partial_x + i\partial_y)\hat{f}_{k-1} = \lambda(P_{0,k} - 1)\hat{f}_k + \sum_q I_{q,k}\hat{f}_q \hat{f}_{k-q} \,. \tag{3.34}$$

3.4 Dimensionless variables

It is convenient to remove dimensions from the equations, i.e. to measure quantities in units given by suitable combinations of the parameters defining our model. For this purpose we define new dimensionless variables (and rename them with the original label for simplicity)

$$\begin{cases} \tilde{t} = \lambda t \to t \quad (time) \\ \tilde{x} = \lambda x / v_0 \to x \quad (space) \\ \tilde{f} = f/\rho \to f \quad ([density] = 1/m^2) \,. \end{cases}$$

Recalling the dimensions of the cross section from Eq. (3.11), we also make the following choice [17]

$$\hat{\rho} = \rho d v_0 / \lambda = 1 \tag{3.35}$$

which means measuring density by the inverse of the area that the diameter of a particle spans between two diffusion events (λ is in fact the diffusion rate).

Employing this scheme the dimensionless equation for the Fourier modes reads

$$\partial_t \hat{f}_k + \frac{1}{2}\nabla^* \hat{f}_{k+1} + \frac{1}{2}\nabla \hat{f}_{k-1} = (P_{0,k} - 1)\hat{f}_k + \sum_{q=-\infty}^{\infty} I_{q,k}\hat{f}_q \hat{f}_{k-q} \,, \tag{3.36}$$

with the definition of the complex operator $\nabla := \partial_x + i\partial_x$ and its complex conjugate $\nabla^* := \partial_x - i\partial_y$.
The dimensionless integral coefficient is

$$I_{q,k} = \frac{2}{\pi} \int_{-\pi}^{\pi} d\Delta \, |\sin(\Delta/2)| \left[P_k \cos(\Delta(q - \omega k)) - \cos(q\Delta) \right] \,. \tag{3.37}$$

3.5 Boltzmann equation for two species of particles

In this section we want to generalize the Boltzmann equation to a system where two different species of particles are mixed; we will assume that the two can differ by density and diffusion/collision noise. We then have a system of coupled Boltzmann

equations with a completely new term due to the collisions between particles belonging to species A and B respectively. The system of equations in real space reads

$$\begin{cases} A: & \left[\frac{\partial}{\partial t} + v_0 \mathbf{e}_\theta \cdot \frac{\partial}{\partial \mathbf{r}}\right] f^A(\mathbf{r},\theta,t) = I_d^A[f^A] + I_c^A[f^A] + I_c^{A-B}[f^A f^B] \\ B: & \left[\frac{\partial}{\partial t} + v_0 \mathbf{e}_\theta \cdot \frac{\partial}{\partial \mathbf{r}}\right] f^B(\mathbf{r},\theta,t) = I_d^B[f^B] + I_c^B[f^B] + I_c^{B-A}[f^B f^A] \end{cases} \tag{3.38}$$

where both single-species diffusion and collisional integrals look the same as before, just with their respective parameters. The additional term due to inter-species collision has the same form as the previously defined collision integral but it involves both distribution functions and a new collisional noise σ_{A-B}

$$\begin{aligned} I_c^A[f^A f^B] = &-f^A(\theta)\int_{-\pi}^{\pi} d\theta' R^{A-B}(\theta',\theta) f^B(\theta') \\ &+ \int_{-\pi}^{\pi} d\theta_1 d\theta_2 R^{A-B}(\theta_1,\theta_2) f^A(\theta_1) f^B(\theta_2) \\ &\times \int_{-\infty}^{\infty} d\eta P^{A-B}(\eta)\delta_{2\pi}(\bar{\theta}^{A-B} + \eta - \theta)\,. \end{aligned} \tag{3.39}$$

As before we expand the distribution functions in Fourier modes:

Species A

$$\begin{aligned} \partial_t \hat{f}_k^A + \frac{1}{2} v_0 \nabla^* \hat{f}_{k+1}^A + \frac{1}{2} v_0 \nabla \hat{f}_{k-1}^A = &\lambda(P_{0,k}^A - 1)\hat{f}_k^A \\ &+ \sum_{q=-\infty}^{\infty} (I_{q,k}^{A-A} \hat{f}_q^A \hat{f}_{k-q}^A + I_{q,k}^{A-B} \hat{f}_q^A \hat{f}_{k-q}^B) \end{aligned} \tag{3.40}$$

Species B

$$\begin{aligned} \partial_t \hat{f}_k^B + \frac{1}{2} v_0 \nabla^* \hat{f}_{k+1}^B + \frac{1}{2} v_0 \nabla \hat{f}_{k-1}^A = &\lambda(P_{0,k}^B - 1)\hat{f}_k^B \\ &+ \sum_{q=-\infty}^{\infty} (I_{q,k}^{B-B} \hat{f}_q^B \hat{f}_{k-q}^B + I_{q,k}^{B-A} \hat{f}_q^B \hat{f}_{k-q}^A) \end{aligned} \tag{3.41}$$

with

$$I_{q,k}^A = \int_{-\pi}^{\pi} \frac{d\Delta}{2\pi} R^A(\Delta) \left[P_k^A \cos(\Delta(q-\omega k)) - \cos(q\Delta)\right] \tag{3.42}$$

$$I_{q,k}^{A-B} = \int_{-\pi}^{\pi} \frac{d\Delta}{2\pi} R^{A-B}(\Delta) \left[P_k^{A-B} \cos(\Delta(q-\omega k)) - \cos(q\Delta)\right]\,. \tag{3.43}$$

The same holds for species B with its own parameters, just by exchanging $A \Leftrightarrow B$. In our derivation we have applied the same nondimensionalization scheme as in Eq. (3.4) for each one of the two distributions.
Furthermore we set $\rho_A \frac{d_A v_A}{\lambda_A} = 1$ and $\rho_B \frac{d_B v_B}{\lambda_A}$.

Throughout the whole discussion on binary mixtures, we will consider collisional and diffusion noise to be equal within each single species

$$\sigma_A = \sigma_{d,A} = \sigma_{c,A} \tag{3.44}$$
$$\sigma_B = \sigma_{d,B} = \sigma_{c,A}\,. \tag{3.45}$$

The inter-species collisional noise will be set equal to the average of the two

$$\sigma_{A-B} = \frac{1}{2}(\sigma_A + \sigma_B)\,. \tag{3.46}$$

3.6 Zero mode equation

According to Eq. (3.12) the $k = 0$ mode coincides with the particle density and its evolution equation reads

$$\partial_t \hat{f}_0^A + \frac{1}{2}\nabla^* \hat{f}_1^A + \frac{1}{2}\nabla \hat{f}_{-1}^A = 0\,, \tag{3.47}$$

since $I_{q,0}^{A-A} = I_{q,0}^{A-B} = 0$ and $P_{0,0}^A = 1$.
Observing that f is a real-valued function so that $\hat{f}_k^A = (\hat{f}_{-k}^A)^*$ and that $\hat{f}_0^A = \rho^A$ Eq. (3.47) reads

$$\partial_t \rho^A + \frac{1}{2}\nabla^* \hat{f}_1^A + \frac{1}{2}\nabla (\hat{f}_1^A)^* = 0\,, \tag{3.48}$$

which is the typical form of a continuity equation if we map vectors of the plane onto complex numbers. Note that in Eq. (3.48) no coupling due to inter-species collisions is present. This appears only in the evolution equation for the first mode.

3.7 First mode equation

$$\partial_t \hat{f}_1^A + \frac{1}{2}\nabla^* \hat{f}_2^A + \frac{1}{2}\nabla \hat{f}_0^A = (P_{0,1}^A - 1)\hat{f}_1^A + \sum_{q=-\infty}^{\infty} (I_{q,1}^{A-A} \hat{f}_q^A \hat{f}_{1-q}^A + I_{q,1}^{A-B} \hat{f}_q^A \hat{f}_{1-q}^B), \tag{3.49}$$

where $P_{0,1}^A = e^{-\sigma_A^2/2}$.

From Eq. (3.49) it is clear that ($\hat{f}_0^A = const. = \rho_0$, $\hat{f}_k^A = 0 \ \forall k \geqslant 1$) is a *homogeneous and isotropic solution* or fixed point of Eq. (3.49).
We will refer to it as the Homogeneous-Isotropic-Phase (HIP).
Since Eq. (3.49) involves an infinite sum, it is impossible to find a close set of equations for the Fourier modes and hence a general solution for the problem. This is obviously a consequence of the Fourier expansion of the density function. This means that we must eventually rely on truncation schemes: as customary in this kind of problems we will first try to extract some interesting information by linearising the equations around the fixed point.

We will thus focus on the (space-homogeneous) perturbation of the HIP, considering only $\mathcal{O}(\delta \hat{f}_1^A)$ terms in Eq. (3.49).

4 Linear Stability Analysis

Now that we have found a stationary and homogeneous solution of Eq. (3.49), we are particularly interested in its stability against small perturbations. It is a well known fact that nonequilibrium systems exhibit instability regions of isotropic solutions in parameter space, where many different patterns could arise [55]. This is a very general approach that usually consists of two steps: linearization of the equation of motion around the fixed point and analysis of the eigenvalues (eigenvectors) arising from the first order linear system [13, 46]. With such a procedure we will be able to derive the phase diagram for a binary mixture [1, 30, 33] for uniform perturbation of the HIP and to analyse the dispersion relation in the case of wave-like perturbations [6, 13, 17, 29].

4.1 Homogeneous perturbation of the homogeneous and isotropic phase

The simplest form of linear analysis is the one were the small displacement around the critical point are space independent, i.e. they have infinite wavelength. In this section we retain first order terms in the perturbation of the HIP solution $\rho_A = const$, $\rho_B = const$, $\hat{f}_1^A = 0$, $\hat{f}_1^B = 0$ and study the eigenvalues problem for the Jacobian matrix.
Eq. (3.49) linearised in the homogeneous perturbation reads

$$\begin{aligned}\partial_t \hat{f}_1^A = &(e^{-\sigma_A^2/2} - 1)\hat{f}_1^A \\ &+ (I_{0,1}^{A-A}\hat{f}_0^A\hat{f}_1^A + I_{0,1}^{A-B}\hat{f}_0^A\hat{f}_1^B) \\ &+ (I_{1,1}^{A-A}\hat{f}_1^A\hat{f}_0^A + I_{1,1}^{A-B}\hat{f}_1^A\hat{f}_0^B)\end{aligned} \tag{4.1}$$

and in addition to the single species terms it contains inter-species coupling terms that will largely modify the single-species phase diagram [6].
The linear system of equations for both species is

$$\partial_t \begin{pmatrix} \hat{f}_1^A \\ \\ \hat{f}_1^B \end{pmatrix} = \mathbf{J} \begin{pmatrix} \hat{f}_1^A \\ \\ \hat{f}_1^B \end{pmatrix} \tag{4.2}$$

where the first column of the linearisation matrix $\mathbf{J}$ is (and the other is obtained simply swapping $A \Leftrightarrow B$)

$$\begin{aligned}\mathbf{J}_{1,1} &= e^{-\sigma_A^2/2} - 1 + (I_{0,1}^{A-A}\rho^A + I_{1,1}^{A-A}\rho^A + I_{1,1}^{A-B}\rho^B) \\ \mathbf{J}_{1,2} &= I_{0,1}^{A-B}\rho^A.\end{aligned} \tag{4.3}$$

We would like to stress the fact that $\hat{f}_1$ is a complex field, so that if we want to relate it to the two-dimensional momentum vector we should always refer to its real (x component) and imaginary (y component) part.

Comparing Eq. (4.1) to the linearised equation derived from the hydrodynamic equations by Bertin *et al.* [6, 7, 37] we observe that two additional terms are present:

$$I_{1,1}^{A-B}\rho^B \tag{4.4}$$

that couples the momentum field of species A to the density of species B via the $I_{1,1}^{A-B}$ coefficient, and

$$I_{0,1}^{A-B}\rho^A \tag{4.5}$$

that instead couples $\hat{f}_1^A$ to f_1^B via the density-dependent coefficient $I_{0,1}^{A-B}\rho^A$. The form of these two integrals is the same, independent of the species

$$\begin{aligned} I_{0,1} &= \frac{2}{\pi}\int_{-\pi}^{\pi} d\Delta\, |\sin(\Delta/2)|\,[P_1\cos(\Delta/2) - 1] \\ &= \frac{4}{\pi}\int_{0}^{\pi} d\Delta \sin(\Delta/2)\left[e^{-\sigma_A^2/2}\cos(\Delta/2) - 1\right] \\ &= \frac{4}{\pi}\left(e^{-\sigma_A^2/2} - 2\right) \end{aligned} \tag{4.6}$$

where we have used the parity of the cosine function and the fact that the sine is positive between 0 and π.

$$\begin{aligned} I_{1,1} &= \frac{2}{\pi}\int_{-\pi}^{\pi} d\Delta\, |\sin(\Delta/2)|\,[P_1\cos(\Delta/2) - \cos(\Delta)] \\ &= \frac{4}{\pi}\int_{0}^{\pi} d\Delta \sin(\Delta/2)\left[e^{-\sigma_A^2/2}\cos(\Delta/2) - \cos\Delta\right] \\ &= \frac{4}{\pi}\left(e^{-\sigma_A^2/2} + 2/3\right) \end{aligned} \tag{4.7}$$

4.1.1 The limit of two identical species

As a preliminary check of our linearisation scheme, we want to obtain system of two identical species of particles and thus reproduce the same transition density and phase diagram (σ vs ρ) as in [6]. For this reason we set

$$\begin{aligned} &\sigma_A = \sigma_B = \sigma \\ &\rho_A = \rho_B = \rho \\ &\sigma_{A-B} = \frac{1}{2}(\sigma_A + \sigma_B) = \sigma\,. \end{aligned} \tag{4.8}$$

The two species are now effectively the same, the only difference being a factor 2 in front of the density, due to the fact that now the number of particles has doubled.

The matrix **J** reduces to

$$\begin{pmatrix} e^{-\sigma^2/2} - 1 + \rho(I_{0,1} + 2I_{1,1}) & I_{0,1}\rho \\ I_{0,1}\rho & e^{-\sigma^2/2} - 1 + \rho(I_{0,1} + 2I_{1,1}) \end{pmatrix} \tag{4.9}$$

where all the subscripts referring to the two different species have been removed. To obtain the correct phase diagram we have to pay attention to the form of the matrix

$$\mathbf{J} \sim \begin{pmatrix} a+b & b \\ b & a+b \end{pmatrix} \tag{4.10}$$

where $b = I_{0,1}\rho < 0$. The two eigenvalues are respectively $\lambda_1 = a$, $\lambda_2 = a + 2b$, so that the larger eigenvalue would be λ_1. However if we look at the eigenvectors we find that the one associated with λ_1 is

$$v_1 = \begin{pmatrix} 1 \\ -1 \end{pmatrix} \tag{4.11}$$

which has no physical meaning since a small positive perturbation (say Re$f > 0$ so that the system is perturbed in the positive x direction) would give both a positive and a negative contribution to the polar field. This cannot happen since we are dealing with a single species and the behaviour must be unique. The correct eigenvector to consider is then $(1, 1)^T$, corresponding to the second eigenvalue $\lambda_2 = a + 2b$.

The condition $\lambda_2 = 0$ gives the same transition line as obtained analytically in [6] (a part from a factor of 2 due to the double amount of total particles in the system)

$$\rho_t = \frac{1 - e^{-\sigma^2/2}}{2(I_{0,1} + I_{1,1})} \tag{4.12}$$

Fig. 7 is the phase diagram for the single species system [6, 7, 8, 10, 47, 48]: the region of "high noise" above the transition line is where the homogeneous and isotropic solution is stable (i.e. $\lambda_2 < 0$). The lower part of the (σ, ρ) phase plane, is the *ordered* region, where the homogeneous and isotropic phase becomes unstable and polar order is predicted to arise ($\lambda_2 > 0$).

One of the main features of this phase diagram is that the transition line is always an increasing function of the density, so that a disorder-order transition is possible either via increasing the density or via decreasing the noise. It is a general property of these self-propelled particle systems that by increasing the density the system moves toward order, whereas an increase in noise drives the system away from it [22, 36].

It is also worth noting that $\rho_t(\sigma = 0) = 0$ and that the curve has a divergent derivative at the origin: this means that in the limit of infinitesimally small noise,

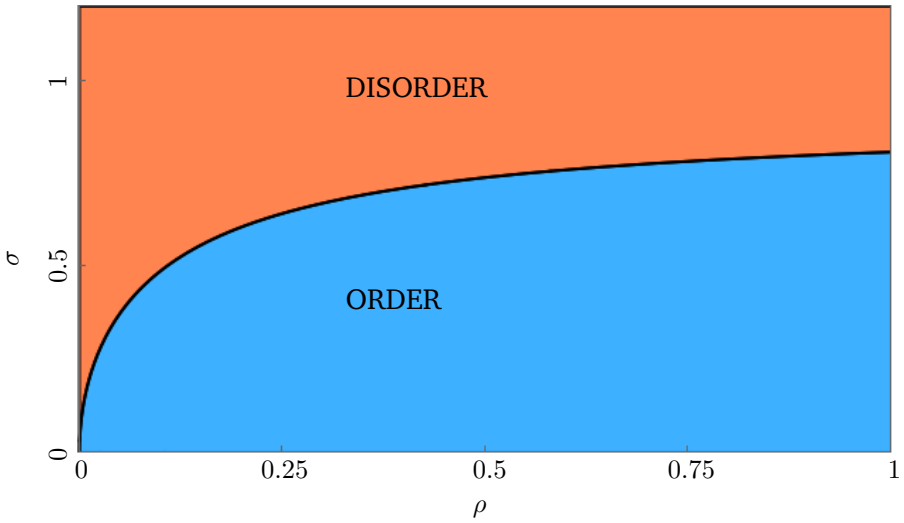

Figure 7: *Orange*: stability region of the HIP ($\hat{f}_0^A = const,\ \hat{f}_k^A = 0\ \forall k \geqslant 1$). *Blue*: instability region of the HIP. In *black* is the transition line Eq. (4.12).

an infinitesimal increase in density would lead to an immediate transition towards order. We can understand this behaviour simply realizing that reducing to zero the noise means that our particles follow a ballistic motion (i.e. they move on a line with constant speed) and they align perfectly with each other (without any "fuzziness" in the outgoing angle) when they collide. We will see that most of these features change substantially when we introduce another species into the system.

4.1.2 The binary case

We will here analytically calculate the general form for the eigenvalues of the matrix **J** and find the conditions for the onset of instabilities in the homogeneous-isotropic state. As already remarked the inter-species collisions yield another addictive term on the diagonal ($I_{1,1}^{A-B}\rho^B$), but also an off diagonal one ($I_{0,1}^{A-B}\rho^A$).
We would intuitively expect that the introduction of a new species with low noise (i.e. ordered) would increase polar order in the system, whereas introducing a really "noisy" second species would promote a disordered stationary state.

For simplicity we will rewrite the matrix **J** in the form

$$\mathbf{J} = \begin{pmatrix} S_A + I_{1,1}\rho^B & I_{0,1}\rho^A \\ I_{0,1}\rho^B & S_B + I_{1,1}\rho^A \end{pmatrix} \tag{4.13}$$

where for the sake of brevity $S_A = e^{-\sigma_A^2/2} - 1 + (I_{0,1}^{A-A} + I_{1,1}^{A-A})\rho^A$ is the single species component and the cross-collision terms are $I_{1,1}$ and $I_{0,1}$. To be consistent with our

previous notation, we remark that $S_A > 0$ implies $\rho^A > \rho_t^A = (1 - P_{0,1}^A)/(I_{0,1}^A + I_{1,1}^A)$ so that species A is in the ordered region (the same holds for B).

The two eigenvalues of the matrix $\mathbf{J}$ read

$$\lambda_{1,2} = (S_A + I_{1,1}\rho^B) + (S_B + I_{1,1}\rho^A) \pm \sqrt{[(S_A + I_{1,1}\rho^B) + (S_B + I_{1,1}\rho^A)]^2 - 4[(S_A + I_{1,1}\rho^B)(S_B + I_{1,1}\rho^A) - I_{0,1}^2\rho^A\rho^B]}\,. \tag{4.14}$$

The expression under the square root sign is always positive so that the *eigenvalues are real*.
Before choosing the correct eigenvalue describing the system, we look first at the associated eigenvectors: for this purpose we indicate with $(\lambda_1, \mathbf{e}_1)$ the pair eigenvalue-eigenvector, λ_1 being given by Eq. (4.14) with the "+" sign. Similarly we take λ_2 to be the eigenvalue with the "−" sign and $\mathbf{e}_2$ the corresponding eigenvector. The exact expression for the two vectors is complicated and not really helpful to get an idea of the behaviour we can easily plot the vector space associated with each eigenvector.

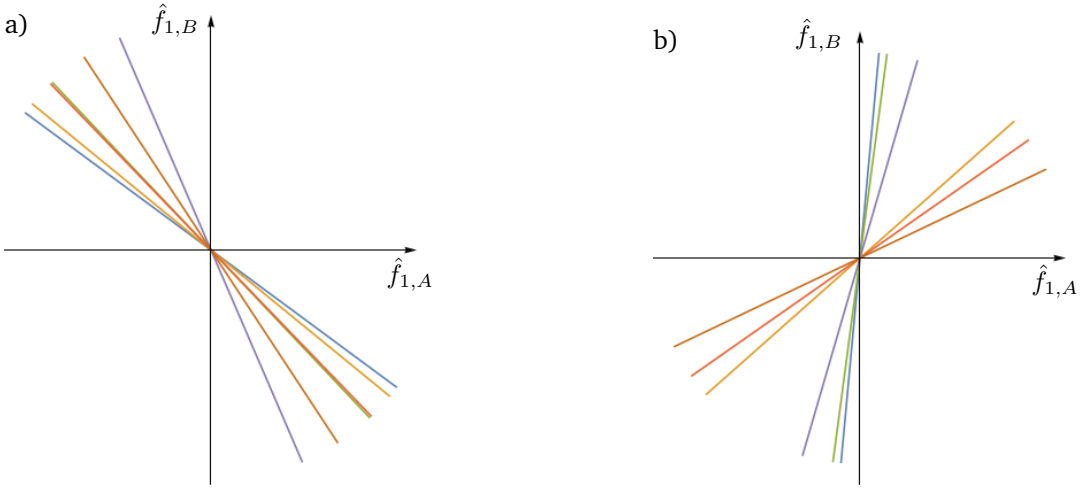

Figure 8: *Left*: various vector spaces associated to the pair $(\lambda_1, \mathbf{e}_1)$ for different values of the noise σ_B. *Right*: vector spaces associated to $(\lambda_2, \mathbf{e}_2)$.

It is clear from Fig. 8 a) that the first eigenvector is of the form

$$\mathbf{e}_1 = \begin{pmatrix} + \\ - \end{pmatrix} \tag{4.15}$$

and lies in the second and in the fourth quadrant, while the second one lies in the first and in the third one

$$\mathbf{e}_2 = \begin{pmatrix} + \\ + \end{pmatrix}. \tag{4.16}$$

In Fig. 9 a) and b) we have drawn a polar and an antipolar collision between polar rods, indicating the two eigen-directions given by $\mathbf{e_1}$ and $\mathbf{e}_2$. If we chose $\mathbf{e}_1$ to describe our system, it is clear from Fig. 9 b) that this would mean enhancing an alignment in the antipolar direction, whereas our collision rule is a polar one.
We then claim that our linearized system is described by

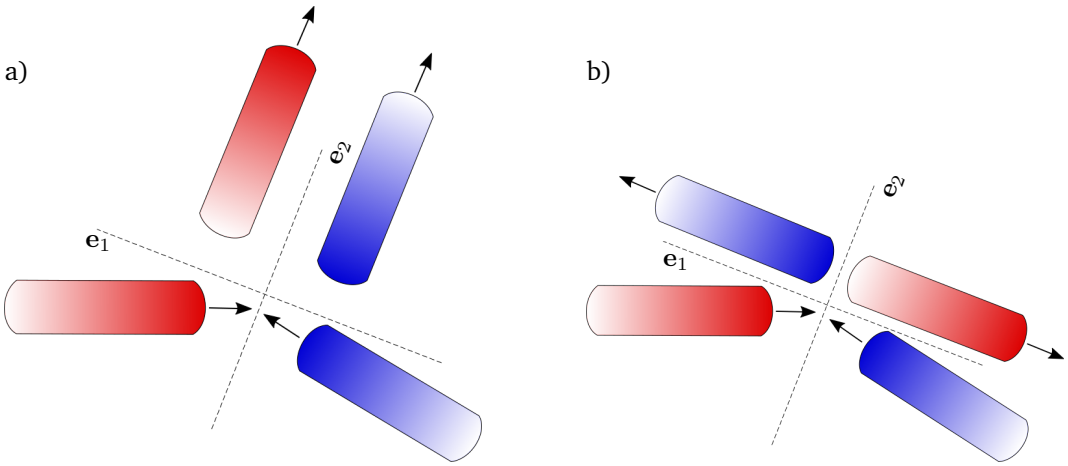

Figure 9: *Left*: collision with polar component only.
Right: collision with antipolar component only.
Dashed: the two orthogonal directions given by the eigenvectors. An alignment along $\mathbf{e_1}$ enhances the *antipolar* component of the momentum, whereas an alignment along $\mathbf{e}_2$ favours the *polar* component consistently with our choice of the collision rule.

$$\begin{aligned}\lambda_2 = &(S_A + I_{1,1}\rho^B) + (S_B + I_{1,1}\rho^A) \\ &- \sqrt{[(S_A + I_{1,1}\rho^B) - (S_B + I_{1,1}\rho^A)]^2 + 4I_{0,1}^2\rho^A\rho^B}\end{aligned} \tag{4.17}$$

$$\mathbf{e}_2 = \begin{pmatrix} + \\ + \end{pmatrix}. \tag{4.18}$$

Eventually, our condition for the instability of the HIP is $\lambda_2 > 0$ or by squaring Eq. (4.17)

$$(S_A + I_{1,1}\rho^B)(S_B + I_{1,1}\rho^A) > I_{0,1}^2\rho^A\rho^B \tag{4.19}$$

that can be plotted while we vary the four different parameters of the system $(\rho_A, \sigma_A, \rho_B, \sigma_B)$.
To obtain a two dimensional phase diagram we have to fix two of these. We choose to fix the density of species B and to plot the phase diagram *for the whole mixture* as a function of the pair (σ_A, ρ_A), while varying σ_B through a prefixed range of discrete values.

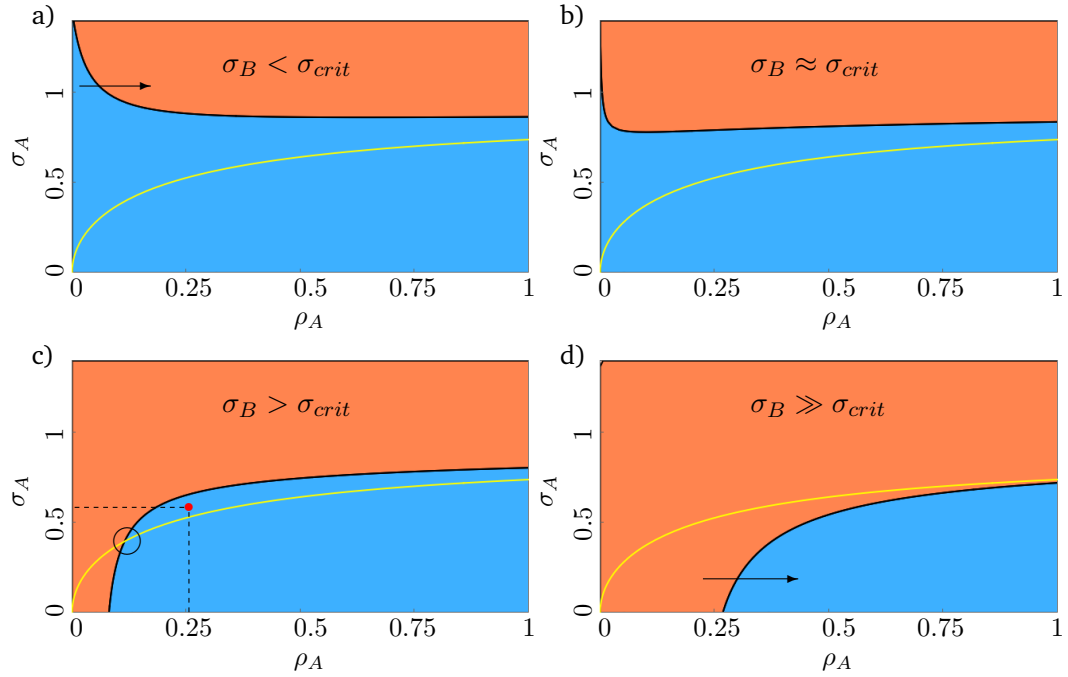

Figure 10: Linear stability phase diagram (of the binary mixture A-B) for four different values of σ_B. In *orange* the disordered region, in *blue* the ordered phase. The new transition line for the binary mixture (i.e. the boundary between the orange and the blue region) is in *black*. For comparison, the single species transition line is plotted in *yellow*. *Black* arrows in a) and d) show possible phase transitions for constant noise and increasing density. The *black circle* in c) points out the crossing of the single species line (yellow) and the one for the binary mixture (black). The *red dot* is a possible choice of parameters for the mixture to be in an ordered state while having already left the single species ordered phase (below the yellow line).

What we obtain is an interesting phase diagram for the two-species system as the noise of species B is increased going from a) to d): order seems to be promoted for noise values *below* the transition line but for high values of the noise the most of our phase diagram is occupied by the disordered phase. Physically this means that if we mix two species, the former (B) being in an *ordered state* and the latter (A) being in a *disordered phase*, we can obtain an *ordered mixture* (see Fig. 10 a)). In this situation a transition from order to disorder (and not viceversa) is possible by *increasing* the density for σ_A large enough (dashed arrow in Fig. 10 a)). This is due to the fact that the transition line is decreasing with density for $\sigma_B < \sigma_{crit}$.

For $\sigma_B \approx \sigma_{crit.}$ the transition line becomes almost horizontal and eventually changes discontinuously its concavity when the critical value is crossed. Looking at Fig 10 b) more carefully it seems that for noise values close to critical an inverse transition disorder-order is possible at high densities: the transition line seems in fact to reach the minimum around $\rho \approx 0.05$ and then to increase. This suggests that

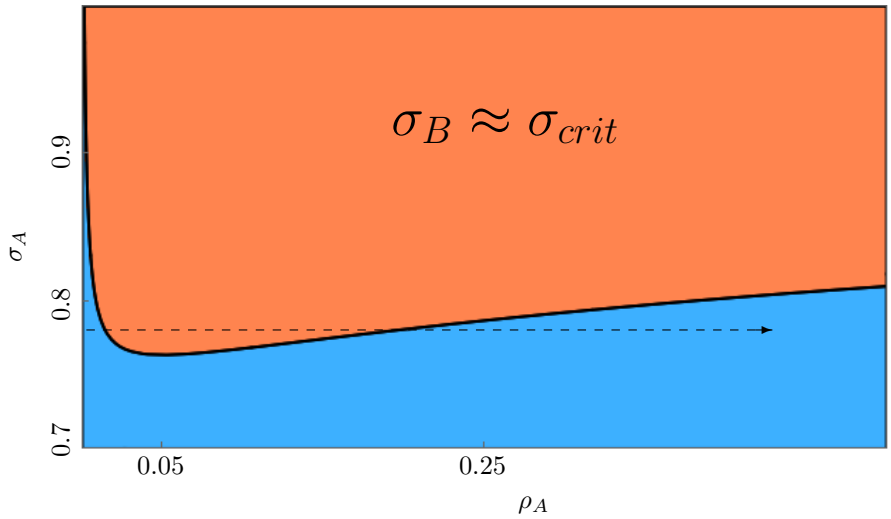

Figure 11: *Zoom of Fig. 10 b)*: close to $\sigma_B = \sigma_{crit}$ the transition curve first decreases towards a minimum and then increases again. The arrow indicates the possibility of a re-entrant phase transition for $\sigma_A \approx 0.78$. Here $\rho_B = 0.4$ and $\sigma_B = 0.605 \lesssim \sigma_{crit}$.

a mixture with parameters tuned in the correct way would exhibit first an order-disorder transition and then a disorder-order one as shown by the dashed arrow in Fig. 11; such a behaviour is usually called "re-entrant" [41].

Moreover, according to our phase diagram it is possible to obtain an ordered system by mixing two *disordered* ensembles of particles: this is shown in Fig. 10 c) where we observe that the single-species transition line (in yellow) crosses the new one (in black). Thus if we choose our parameters (cf. the red point in Fig. 10 c)) so that the system is *above* the yellow line but *below* the black one, we end up with an ordered mixture, despite the two separate species being singularly *above* their transition line and thus disordered [1, 30].

In Fig. 10 d) the noise is way above criticality and the two transition lines don't cross each other any more (for densities smaller than one). The new *density threshold* that appears around $\rho_A \approx 0.25$ for $\sigma_B \gg \sigma_{crit}$ (Fig. 10) is another interesting feature: the density of species A always has to overcome a certain value for the system to be ordered. Again a comparison with the single species case shows that the yellow line always starts from the origin and such a threshold is not present.

Remarkably, our results are in agreement with what Ariel *et al.* found simulating a binary mixture via a slightly modified SNM (Scalar Noise Model) [1, 54]. In particular their phase diagrams (cf. Fig. 4,5 and 6 of Ref. [1]) qualitatively shows the same features as our linearised Boltzmann approach does: order is promoted and even a density threshold for σ_B larger than the critical value (Fig. 10 d)) indirectly appears. By indirectly we mean that they don't explicitly point out a particular value

that has to be overcome to promote order, but a careful comparison between Fig. 4 and 6 of Ref. [1] and our phase diagrams Fig. 10 shows that this is indeed the case.

We obviously obtain the same results if instead of fixing the density of species B we fix the noise and move horizontally to larger values of the density crossing the "single-species" transition line.

4.2 Non-homogeneous perturbation of the homogeneous and isotropic phase

Until now we have investigated the stability of the homogeneous-isotropic phase against homogeneous perturbations. However we didn't look at how our system reacts to small finite-wavelength perturbations of the HIP [32]. Patterns could in fact arise if we perturb the uniform state of the system with small but now space-dependent variations of our fields. We recall that in our homogeneous linear stability analysis we found two distinct regions in phase space: one where perturbations of the HIP decay exponentially (thus stable) and one where those instabilities grow exponentially. In this section of the thesis we investigate if this is also true when tiny perturbations of the form $e^{\lambda t}e^{i\mathbf{q}\cdot\mathbf{x}}$ are introduced. In Fig. 12 the dispersion relation for a type-III instability is drawn: on the y-axis lies the real part of the eigenvalue, while on the x-axis the magnitude of $\mathbf{q}$. Typically the system depends on a few important parameters (in our case density and noise) that can modify the stability diagram. In particular we see that a critical value of the density ρ_c indicates the onset of instability; in other words for $\rho > \rho_c$ there are values of q for which $Re(\lambda)$ is positive and the system becomes unstable. The fastest growing mode is the one for which the growth rate λ is maximum and for a III-type instability it is always the $q = 0$ one. In our specific case (that will not exhibit a type-III instability) the control parameter is the critical density (or noise) for the binary mixture. For the sake of brevity, we will from now on drop the "hat" symbol as well as the "1st order" subscript of the first Fourier mode and when substituting into equations we don't indicate dependencies any more.

We rewrite our fields in the following way, emphasizing the small perturbations around the fixed point

$$\rho^A(\mathbf{r},t) = \rho_0^A + \delta\rho^A(\mathbf{r},t), \quad f^A(\mathbf{r},t) = \delta f^A(\mathbf{r},t) \tag{4.20}$$

$$\rho^B(\mathbf{r},t) = \rho_0^B + \delta\rho^B(\mathbf{r},t), \quad f^B(\mathbf{r},t) = \delta f^B(\mathbf{r},t) \tag{4.21}$$

and we substitute into Eq. (3.48) and Eq. (3.49) for species A and B respectively. Considering again only order one in the perturbations (and their complex conjugates), we obtain

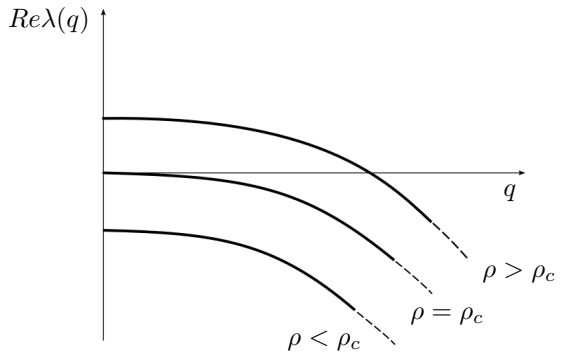

Figure 12: Example of a dispersion relation for a type-III instability. The maximum of Re$\lambda(q)$ occurs always at $q = 0$. For $\rho > \rho_c$ spatial instabilities arise, while for $\rho \leq \rho_c$ the fixed point is stable.

Species A

$$\partial_t \delta\rho^A + \frac{1}{2}\nabla^* \delta f^A + \frac{1}{2}\nabla(\delta f^A)^* = 0 \tag{4.22}$$

$$\partial_t \delta f^A + \frac{1}{2}\nabla \delta\rho^A = (P^A_{0,1} - 1 + I^{AA}_{0,1}\rho^A_0 + I^{AA}_{1,1}\rho^A_0 + I^{AB}_{1,1}\rho^B_0)\delta f^A + I^{AB}_{0,1}\rho^A_0 \delta f^B \,. \tag{4.23}$$

Species B

$$\partial_t \delta\rho^B + \frac{1}{2}\nabla^* \delta f^B + \frac{1}{2}\nabla(\delta f^B)^* = 0 \tag{4.24}$$

$$\partial_t \delta f^B + \frac{1}{2}\nabla \delta\rho^B = (P^B_{0,1} - 1 + I^{BB}_{0,1}\rho^B_0 + I^{BB}_{1,1} f^B_0 + I^{BA}_{1,1}\rho^A_0)\delta f^B + I^{BA}_{0,1}\rho^B_0 \delta f^A \,. \tag{4.25}$$

Two more equations for the two complex conjugate fields $(\delta f^A)^*$ and $(\delta f^B)^*$ need to be added to complete the linear system: they can be easily obtained by taking the complex conjugate of the corresponding Eq. (4.23), Eq. (4.25) paying attention to the complex nabla operators.
The ansatz we will make for the perturbation is a *plane-wave* one, namely

$$\delta\rho(\mathbf{r}, t) = \sum_{\mathbf{q}} \delta\rho_{\mathbf{q}}(t) \quad e^{i\mathbf{q}\cdot\mathbf{r}} \quad \delta f(\mathbf{r}, t) = \sum_{\mathbf{q}} \delta f_{\mathbf{q}}(t)\, e^{i\mathbf{q}\cdot\mathbf{r}} \,, \tag{4.26}$$

where the wave vector $\mathbf{q}$ is real whether the amplitudes $\delta\rho_{\mathbf{q}}(t)$, $\delta f_{\mathbf{q}}(t)$ are complex and their modulus is assumed to be small. We recall that the time-dependent

amplitudes can be obtained using the relations

$$\delta f_{\mathbf{q}'}(t) = \frac{1}{2\pi}\int d\mathbf{r}\,\delta f(\mathbf{r},t)e^{-i\mathbf{q}'\cdot\mathbf{r}}\,, \tag{4.27}$$

$$\delta \rho_{\mathbf{q}'}(t) = \frac{1}{2\pi}\int d\mathbf{r}\,\delta \rho(\mathbf{r},t)e^{-i\mathbf{q}'\cdot\mathbf{r}}\,, \tag{4.28}$$

for the first moment and the density respectively. If we now substitute our expressions into the three equations for species A and for species B, we can derive the linear evolution equations for the amplitudes $\delta f_{\mathbf{q}}(t) \sim \delta f_{\mathbf{q}} e^{\lambda_{\mathbf{q}} t}$ and $\delta \rho_{\mathbf{q}}(t) \sim \delta \rho_{\mathbf{q}} e^{\lambda_{\mathbf{q}} t}$. By choosing the correct eigenvalue for the system we can then find the dispersion relation and study for which values of the noise, instability occurs.

The linear system reads

$$\partial_t \begin{pmatrix} \delta\rho^A \\ \delta\rho^B \\ \delta f^A \\ \delta f^{A*} \\ \delta f^B \\ \delta f^{B*} \end{pmatrix} = \mathbf{J}(\mathbf{q}) \begin{pmatrix} \delta\rho^A \\ \delta\rho^B \\ \delta f^A \\ \delta f^{A*} \\ \delta f^B \\ \delta f^{B*} \end{pmatrix}\,, \tag{4.29}$$

the rows of the linearisation matrix being given for $(j = 1, \cdots, 6)$ by

$$\mathbf{J}_{1,j} = \left(0,\, 0,\, -\frac{1}{2}(iq_x + q_y),\, \frac{1}{2}(iq_x - q_y),\, 0,\, 0\right)\,,$$

$$\mathbf{J}_{2,j} = \left(0,\, 0,\, 0,\, 0,\, -\frac{1}{2}(iq_x + q_y),\, \frac{1}{2}(iq_x - q_y)\right)\,,$$

$$\mathbf{J}_{3,j} = \left(-\frac{1}{2}(iq_x - q_y),\, 0,\, (P^A_{0,1} - 1) + (I^{AA}_{0,1} + I^{AA}_{1,1})\rho^A_0 + I^{AB}_{1,1}\rho^B_0,\, 0,\, I^{AB}_{0,1}\rho^A_0,\, 0\right)\,,$$

$$\mathbf{J}_{4,j} = \left(+\frac{1}{2}(iq_x + q_y),\, 0,\, 0,\, (P^A_{0,1} - 1) + (I^{AA}_{0,1} + I^{AA}_{1,1})\rho^A_0 + I^{AB}_{1,1}\rho^B_0,\, 0,\, I^{AB}_{0,1}\rho^A_0\right)\,,$$

$$\mathbf{J}_{5,j} = \left(0,\, -\frac{1}{2}(iq_x - q_y),\, I^{BA}_{0,1}\rho^B_0,\, 0,\, (P^B_{0,1} - 1) + I^{BB}_{0,1}\rho^B_0 + I^{BB}_{1,1}f^B_0 + I^{BA}_{1,1}\rho^A_0,\, 0\right)\,,$$

$$\mathbf{J}_{6,j} = \left(0,\, +\frac{1}{2}(iq_x + q_y),\, 0,\, I^{BA}_{0,1}\rho^B_0,\, 0,\, (P^B_{0,1} - 1) + I^{BB}_{0,1}\rho^B_0 + I^{BB}_{1,1}f^B_0 + I^{BA}_{1,1}\rho^A_0\right)\,.$$

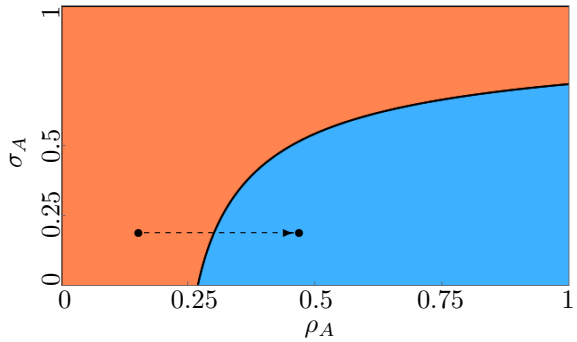

Figure 13: *Dashed line*: the dispersion relation Re$\lambda(q)$ is evaluated for two different points on the phase diagram, connected by a line. The one on the right side of the transition line is in the stable regime, the other in the unstable. $\rho_B = 0.4$, $\sigma_B = 0.9$.

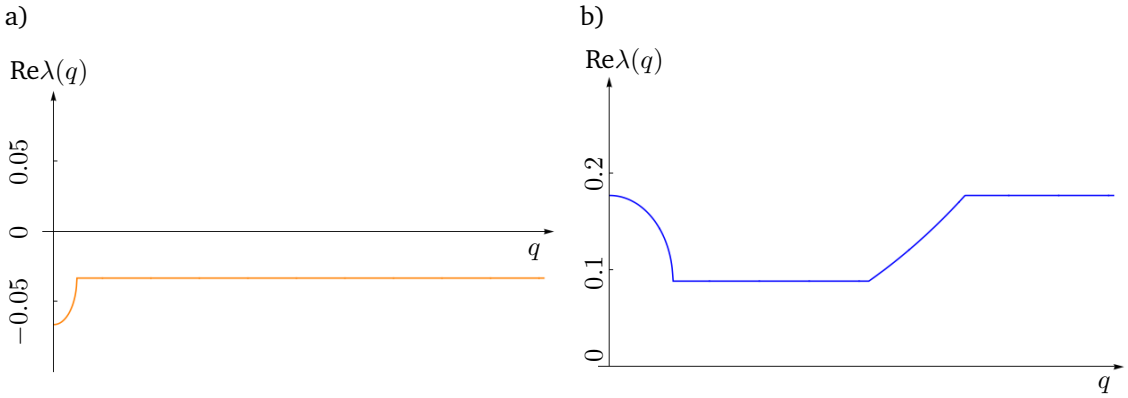

Figure 14: *Left:* dispersion relation for non-homogeneous perturbation of the HIP in the *orange* region (Fig. 13). The real part of the eigenvalue is always negative, thus confirming the stability of the fixed point.
Right: dispersion relation for non-homogeneous perturbation of the HIP in the *blue* region (Fig. 13). Here the eigenvalue's real part is always positive, indicating that the homogeneous and isotropic state is always unstable against wave-like perturbations.

Despite the analytic expression for each eigenvalue being too complicated, we can numerically diagonalize the matrix and plot the results for different values of the parameters as we have done in the homogeneous case. Similarly to what we did in Sect. 4.1.2 we look for the eigenvector "compatible" with our model and plot the corresponding eigenvalue. For symmetry reasons, the dispersion relation depends only on the magnitude of the wave vector $|\mathbf{q}| = q$.
In order to relate our analytical results to the numerical ones that we will present in Sect. 6.2, we vary ρ_A along the dashed arrow shown in Fig. 13, while keeping $\sigma_B = 0.9$, $\rho_B = 0.4$. As before, by varying the noise of species B we can change the stability of a specific region: in orange is the disordered state, in blue the ordered one. In Fig. 14 a) the dispersion relation for the point in the *orange* region is displayed: for non homogeneous perturbations, the real part of the eigenvalue is negative through the whole q range. We can then conclude that this region of the phase diagram $\rho_A < \rho_{crit}$ is stable against *homogeneous* ($\lambda_2 < 0$, cf. Sect 4.1) and *inhomogeneous* perturbations for all values of q [3, 6, 7, 32]. Moving across the dashed line of Fig. 13 we enter the blue region where our homogeneous linear stability analysis returned a positive eigenvalue, indicating that

the HIP is here unstable ($\lambda_2 > 0$). Fig. 14 b) tells us that here also space-dependent perturbations grow exponentially, for all values of q. In addition, note that for $q \neq 0$ the growth rate λ first decreases then stays constant and eventually increases again to reach the same value as for $q = 0$. All the kinks present in Fig. 14 are degenerate points where two or more eigenvalues are equal.

After having studied the stability of the trivial homogeneous and isotropic solution of the Boltzmann equation, both against uniform and non uniform perturbations, it is natural to go one step further, try to find another solution of the equations of motion and eventually study its stability. We will deal with the first task in the next section.

5 Hydrodynamic Equations

The advantage of an approach that makes use of the kinetic Boltzmann equation is that it is particularly efficient in relating microscopic quantities like diffusional noise, mean free path, size of particles etc. to macroscopic ones that appear in the statistical description of the system. The approach that we describe now, characterizes the whole system via two macroscopic fields: density $\rho(\mathbf{x}, t)$ and momentum $\mathbf{p}(\mathbf{x}, t)$ or equivalently $f_1(\mathbf{x}, t)$. The nonlinear equations that determine their evolution are called *hydrodynamic equations*. We will see that they are particularly suitable for finding another non trivial fixed point of our binary ensemble and to study its stability, as well as for numerical implementations.
We have already remarked that the nonlinearity of the equations and the presence of an infinite series in Eq. (3.49) don't allow for a general solution of the problem; nevertheless this series form seems well suited for some kind of approximation scheme. The one implemented by Bertin et al. [8] is a possible truncation in order to obtain a (nonlinear) equation for the first mode (or equivalently for the momentum field to which it is related via Eq. (3.17)).
Another way of looking at such an approach is in the spirit of the Ginzburg-Landau theory [37]: the evolution equation for the polar order field can be in general written as

$$\partial_t \hat{f}_1 = \mathcal{G}(\rho, \sigma)\hat{f}_1 \,, \tag{5.1}$$

where $\mathcal{G}$ is a nonlinear operator depending both on the density and on the noise. Close to the onset of instability an expansion of the operator to lowest order in ρ and σ leads to a Ginzburg Landau equation.

In the next section we will shortly recapitulate the procedure conceived in [6], starting from the Fourier transformed Boltzmann equation for a single species of particles. In Sect. 5.2 we derive the hydrodynamic equations for a binary mixture and employ them to find a non isotropic solution (Sec. 5.3).

5.1 Single species case

The underlying assumption of all the following derivation is that the system is in a state which lies very *close to the transition disorder-order* or in other words that the polarization field $\mathbf{P}$ (or also "average velocity") is small compared to the speed of the particles. This quasi-ordered state can be mathematically expressed using the fact that the density is independent from the momentum orientation or $\rho(\mathbf{r}, t) = \mathcal{O}(1)$. We recall that by definition the momentum field is related to $\hat{f}_1$ by $\|\mathbf{p}\| = v_0\rho|\hat{f}_1|$. It follows that if the system is sufficiently close to an isotropic state, i.e. $\|\mathbf{p}\| = \mathcal{O}(\epsilon)$,

we can set

$$\hat{f}_1 = \mathcal{O}(\epsilon), \quad \epsilon \ll 1 \tag{5.2}$$

and since this is the mode that first becomes unstable in a polar system, we imply the following scaling ansatz

$$\hat{f}_k = \mathcal{O}(\epsilon^{|k|})\,. \tag{5.3}$$

Once again it is really important to remember that this approach is only justified close to the transition line.

The first possibility is to retain terms until $\mathcal{O}(\epsilon^3)$, which is the first that accounts for saturation. In [6] this ansatz was verified by numerically computing the spatially homogeneous and stationary solution of the full Boltzmann equation for each k-mode. It is observed that modes with $k \gtrsim 4$ decay exponentially, thus corroborating the hypothesis that the first three modes are sufficient to properly derive the hydrodynamic equations. Furthermore nonlinearities in the polar order field are supposed to saturate at order $\mathcal{O}(\epsilon^3)$, meaning that the coefficients in front of third order terms should be negative. If this is not the case, we need to go to higher orders and assure that there exist values of noise and density such that the coefficient of the lowest-order symmetry-allowed nonlinear term is negative. By applying a third order truncation we can express all $\hat{f}_2$ terms as a function of ρ and $\hat{f}_1$ and successively use this result to substitute into the equation for $\hat{f}_1$, as we will now briefly show.

First of all we write down the evolution equations for the first three moments, as prescribed by Eq. (3.36), to order ϵ^3

$$\partial_t \rho + \nabla \hat{f}_1^* + \nabla^* \hat{f}_1 = 0\,, \tag{5.4}$$

$$\begin{aligned}\partial_t \hat{f}_1 + \frac{1}{2}\nabla^* \hat{f}_2 + \frac{1}{2}\nabla\rho &= (P_{0,1}-1)\hat{f}_1 + I_{0,1}\rho\hat{f}_1 + I_{1,1}\hat{f}_1\rho \\ &+ I_{-1,1}\hat{f}_1^*\hat{f}_2 + I_{2,1}\hat{f}_2\hat{f}_1^*\,,\end{aligned} \tag{5.5}$$

$$\partial_t \hat{f}_2 + \frac{1}{2}\nabla\hat{f}_1 = (P_{0,2}-1)\hat{f}_2 + I_{0,2}\rho\hat{f}_2 + I_{1,2}\hat{f}_1^2 + I_{2,2}\hat{f}_2\rho\,. \tag{5.6}$$

We will consider the second mode $\hat{f}_2$ to have already relaxed to the stationary value, since it varies on a much faster time scale than $\hat{f}_1$, so that we can set $\partial_t \hat{f}_2 = 0$ (for a more rigorous definition of the scaling ansatz see [6, 7, 37]).
Eq. (5.6) then yields

$$\hat{f}_2 = \frac{\frac{1}{2}\nabla\hat{f}_1 - I_{1,2}\hat{f}_1^2}{P_{0,2} - 1 + (I_{0,2}+I_{2,2})\rho}\,. \tag{5.7}$$

Substituting this result into Eq. (5.5) we obtain

$$\partial_t \hat{f}_1 + \frac{1}{2}\nabla^* \left(\frac{\frac{1}{2}\nabla \hat{f}_1 - I_{1,2}\hat{f}_1^2}{P_{0,2} - 1 + (I_{0,2} + I_{2,2})\rho} \right) + \frac{1}{2}\nabla\rho = (P_{0,1} - 1)\hat{f}_1 + I_{0,1}\rho\hat{f}_1 + I_{1,1}\hat{f}_1\rho$$
$$+ I_{-1,1}\hat{f}_1^* \frac{\frac{1}{2}\nabla \hat{f}_1 - I_{1,2}\hat{f}_1^2}{P_{0,2} - 1 + (I_{0,2} + I_{2,2})\rho} + I_{2,1} \frac{\frac{1}{2}\nabla \hat{f}_1 - I_{1,2}\hat{f}_1^2}{P_{0,2} - 1 + (I_{0,2} + I_{2,2})\rho} \hat{f}_1^* \,. \tag{5.8}$$

By defining the coefficients μ and ν

$$\mu(\rho) = P_{0,1} - 1 + (I_{0,1} + I_{1,1})\rho \tag{5.9}$$
$$\nu(\rho) = [P_{0,2} - 1 + (I_{0,2} + I_{2,2})\rho]^{-1} \tag{5.10}$$

we can rewrite Eq. (5.8) in the following way

$$\begin{aligned} &\partial_t \hat{f}_1 + \frac{1}{4}\frac{\partial \nu}{\partial \rho}\nabla^*\rho\,\nabla\hat{f}_1 - \frac{I_{1,2}}{4}\,\nu\,\nabla^2\hat{f}_1 - \frac{I_{1,2}}{2}\,\nu\,\nabla^*\hat{f}_1^2 \\ &= \mu\hat{f}_1 + \frac{I_{-1,1}}{2}\,\nu\,\hat{f}_1^*\,\nabla\hat{f}_1 - \nu I_{-1,1}\hat{f}_1^*\hat{f}_1^2 + \nu\frac{I_{2,1}}{2}\nabla\hat{f}_1\,\hat{f}_1^* - \nu I_{2,1}I_{1,2}\hat{f}_1^2\hat{f}_1^* \,. \end{aligned} \tag{5.11}$$

The system of hydrodynamic equations is then given by Eq. (5.4) and Eq. (5.11) coupled to one another. We could in principle also obtain an equation for the *momentum field* $\mathbf{p}(\mathbf{r}, t)$ defined in Eq. (3.17) that looks more similar to a Navier-Stokes equation where additional terms due to the system being non conservative appear (see for example [6]). We instead highlight the fact that a nontrivial solution of the hydrodynamic equations can be found:

$$\rho = const\,, \quad \hat{f}_1 = const \neq 0\,. \tag{5.12}$$

It is easy to see that if we plug this ansatz into our hydrodynamic equations, Eq. (5.4) reduces to an identity and Eq. (5.11) to

$$\mu\hat{f}_1 - \nu(I_{-1,1} + I_{2,1}I_{1,2})\hat{f}_1^*\hat{f}_1^2 = 0\,. \tag{5.13}$$

Obviously $\hat{f}_1 = 0$ i.e. the isotropic phase is still a solution of Eq. (5.13) but now for $\mu > 0$ we find a second one, namely

$$|\hat{f}_1|^2 = \frac{\mu}{\nu(I_{-1,1} + I_{2,1}I_{1,2})} = \frac{\mu}{\xi}\,, \tag{5.14}$$

where we have defined a new ν (and thus ρ)-dependent coefficient

$$\xi = \frac{8\nu}{15\pi}\left[11 + 15\left(e^{-2\sigma^2} - e^{-\sigma^2/2}\right)\right]\,. \tag{5.15}$$

To conclude, for $\mu > 0$ in addition to the trivial $\rho = const, \quad \hat{f}_1 = 0$ solution a new homogeneous and non-isotropic phase is found, given by $\rho = const, \quad \hat{f}_1 = e^{i\theta}\sqrt{\frac{\mu}{\xi}}$ that corresponds to an average momentum $\mathbf{p}$ with fixed magnitude and general direction θ [6, 7].

5.2 Binary mixture

In a binary system things are more complicated since we have to deal with another nonlinear coupling term due to inter-species collisions. As we will now show, this leads to long and complicated expressions before we can finally reduce the differential system of six equations (modes $0,\ 1,\ 2$ for both species) to four coupled hydrodynamic equations for ρ_A, ρ_B and the two polarization fields f_1^A, f_1^B. Note that for the sake of simplicity we will hereafter drop the "hat" indicating that we are working in Fourier space. The same ansatz as for the single species case is applied, so that terms until order three in epsilon are retained. This is again justified only close to the transition line (of the phase diagram for binary mixtures) and should be proved numerically to be a correct assumption. Furthermore we should once again check that the coefficient of the highest order term (i.e. $\mathcal{O}(\epsilon^3)$) is negative. We will derive the equations for species A but a completely analogous derivation is valid for B.

We start out by writing down the equation for the second Fourier mode f_2^B, where we already discarded the time derivative $\partial_t f_2$ and all higher order terms for the same reasons as in the single species case

$$\begin{aligned} f_2^B\left(I_{0,2}^{BB}\rho_B + I_{2,2}^{BB}\rho_B + I_{2,2}^{BA}\rho_A + P_{0,2}^B - 1\right) = \frac{1}{2}\nabla f_1^B - I_{0,2}^{BA}\rho_B f_2^A \\ - I_{1,2}^{BB}(f_1^B)^2 - I_{1,2}^{BA} f_1^B f_1^A\,. \end{aligned} \tag{5.16}$$

From Eq. (5.16) we can write f_2^B as a function of both densities, of f_1^B, f_1^A and of f_2^A. We then have to substitute this expression into the respective second moment equation for species A to eliminate the field f_2^B

$$\begin{aligned} \frac{1}{2}\nabla f_1^A = (P_{0,2}^B - 1 + I_{0,2}^{AA}\rho_A + I_{2,2}^{AA}\rho_A + I_{2,2}^{AB}\rho_A) f_2^A \\ + I_{1,2}^{AA}(f_1^A)^2 + I_{1,2}^{AB} f_1^B f_1^A \\ + I_{0,2}^{AB}\rho_A\left(\frac{\frac{1}{2}\nabla f_1^B - I_{0,2}^{BA}\rho_B\, f_2^A - I_{1,2}^{BB}(f_1^B)^2 - I_{1,2}^{BA} f_1^B f_1^A}{I_{0,2}^{BB}\rho_B + I_{2,2}^{BB}\rho_B + I_{2,2}^{BA}\rho_A + P_{0,2}^B - 1}\right)\,. \end{aligned} \tag{5.17}$$

We have highlighted in red the terms $\sim f_2^A$ that can be isolated to give an expression where $f_2^A = F^A(\rho_A, \rho_B, f_1^A, f_1^B)$, F being a generic function replacing the complicated expression given here below

$$
\begin{aligned}
& f_2^A \left(I_{0,2}^{AA}\rho_A + I_{2,2}^{AA}\rho_A + I_{2,2}^{AB}\rho_B + P_{0,2}^A - 1 - \frac{I_{0,2}^{AB} I_{0,2}^{BA}\rho_A\rho_B}{I_{0,2}^{BB}\rho_B + I_{2,2}^{BB}\rho_B + I_{2,2}^{BA}\rho_A + P_{0,2}^B - 1} \right) \\
& = \frac{1}{2}\nabla f_1^A - I_{1,2}^{AA}(f_1^A)^2 - I_{1,2}^{AB} f_1^A f_1^B \\
& - I_{0,2}^{AB}\rho_A \left(\frac{\frac{1}{2}\nabla f_1^B - I_{1,2}^{BB}(f_1^B)^2 - I_{1,2}^{BA} f_1^B f_1^A}{I_{0,2}^{BB}\rho_B + I_{2,2}^{BB}\rho_B + I_{2,2}^{BA}\rho_A + P_{0,2}^B - 1} \right) .
\end{aligned}
\tag{5.18}
$$

To simplify Eq. (5.18) we define two coefficients, in analogy to the single species case

$$
\nu^A = \left[I_{0,2}^{AA}\rho_A + I_{2,2}^{AA}\rho_A + I_{2,2}^{AB}\rho_B + P_{0,2}^A - 1 \right]^{-1} \tag{5.19}
$$

$$
\nu^B = \left[I_{0,2}^{BB}\rho_B + I_{2,2}^{BB}\rho_B + I_{2,2}^{BA}\rho_A + P_{0,2}^B - 1 \right]^{-1} \tag{5.20}
$$

and two functions depending on the polar fields

$$
\mathcal{F}^A(f_1^A, f_1^B) = \frac{1}{2}\nabla f_1^A - I_{1,2}^{AA}(f_1^A)^2 - I_{1,2}^{AB} f_1^A f_1^B \tag{5.21}
$$

$$
\mathcal{F}^B(f_1^A, f_1^B) = \frac{1}{2}\nabla f_1^B - I_{1,2}^{BB}(f_1^B)^2 - I_{1,2}^{BA} f_1^B f_1^A . \tag{5.22}
$$

With these new definitions Eq. (5.18) reads

$$
f_2^A = \frac{\nu^A \mathcal{F}^A - I_{0,2}^{AB}\rho_A (\nu^A)^2 \mathcal{F}^B}{1 - \nu^A \nu^B (I_{0,2}^{AB})^2 \rho_A \rho_B} . \tag{5.23}
$$

Having simplified the expression for $\hat{f}_2$, we can write down the equation for f_1^A to order $\mathcal{O}(\epsilon^3)$ highlighting f_2^A and f_2^B terms in red and blue respectively

$$
\begin{aligned}
\partial_t f_1^A + \frac{1}{2}\nabla^* \, f_2^A + \frac{1}{2}\nabla f_0^A = {} & (P_{0,1}^A - 1) f_1^A + (I_{0,1}^{A-A} f_0^A f_1^A + I_{0,1}^{A-B} f_0^A f_1^B) \\
& + (I_{1,1}^{A-A} f_1^A f_0^A + I_{1,1}^{A-B} f_1^A f_0^B) + (I_{-1,1}^{A-A} + I_{2,1}^{A-A}) \, f_2^A \, (f_1^A)^* \\
& + I_{-1,1}^{A-B} (f_1^A)^* \, f_2^B + I_{2,1}^{A-B} \, f_2^A \, (f_1^B)^* .
\end{aligned}
\tag{5.24}
$$

To make explicit the expression $f_2^B = F^B(\rho_A, \rho_B, f_1^A, f_1^B)$, we use Eq. (5.16) with f_2^A being replaced by Eq. (5.23):

$$
\begin{aligned}
f_2^B = \nu^B \Bigg[& \frac{1}{2}\nabla f_1^B - I_{0,2}^{BA}\rho_B \frac{\nu^A \mathcal{F}^A - I_{0,2}^{AB}\rho_A (\nu^A)^2 \mathcal{F}^B}{1 - \nu^A \nu^B (I_{0,2}^{AB})^2 \rho_A \rho_B} \\
& - I_{1,2}^{BB}(f_1^B)^2 - I_{1,2}^{BA} f_1^B f_1^A \Bigg] .
\end{aligned}
\tag{5.25}
$$

From the expressions $f_2^A = F^A(\rho_A, \rho_B, f_1^A, f_1^B)$ and $f_2^B = F^B(\rho_A, \rho_B, f_1^A, f_1^B)$ we can finally derive our equation for f_1^A that contains only the fields ρ_A, ρ_B, f_1^A, f_1^B

$$\begin{aligned}
&\partial_t f_1^A + \frac{1}{2}\nabla^* \left[\frac{\nu^A \mathcal{F}^A - I_{0,2}^{AB}\rho_A(\nu^A)^2\mathcal{F}^B}{1-\nu^A\nu^B(I_{0,2}^{AB})^2\rho_A\rho_B}\right] + \frac{1}{2}\nabla\rho_A = \\
&\mu^A f_1^A + I_{0,1}^{A-B}\rho_A f_1^B + (I_{-1,1}^{A-A} + I_{2,1}^{A-A})(f_1^A)^* \left[\frac{\nu^A \mathcal{F}^A - I_{0,2}^{AB}\rho_A(\nu^A)^2\mathcal{F}^B}{1-\nu^A\nu^B(I_{0,2}^{AB})^2\rho_A\rho_B}\right] \\
&+ I_{-1,1}^{A-B}(f_1^A)^*\nu^B \left[\frac{1}{2}\nabla f_1^B - I_{0,2}^{BA}\rho_B \frac{\nu^A \mathcal{F}^A - I_{0,2}^{AB}\rho_A(\nu^A)^2\mathcal{F}^B}{1-\nu^A\nu^B(I_{0,2}^{AB})^2\rho_A\rho_B}\right. \\
&\left. - I_{1,2}^{BB}(f_1^B)^2 - I_{1,2}^{BA} f_1^B f_1^A\right] + I_{2,1}^{A-B}(f_1^B)^* \left[\frac{\nu^A \mathcal{F}^A - I_{0,2}^{AB}\rho_A(\nu^A)^2\mathcal{F}^B}{1-\nu^A\nu^B(I_{0,2}^{AB})^2\rho_A\rho_B}\right] .
\end{aligned} \tag{5.26}$$

Eq. (5.26) can be rewritten isolating linear, quadratic, cubic terms and those containing gradients of the fields. This is particularly useful if we are interested in finding a spatially uniform solution with non zero polar order fields. For this purpose we introduce new coefficients in front of each term of different order

$$\begin{aligned}
&\partial_t f_1^A = \mu^A f_1^A + \gamma^A f_1^B + \alpha^A(\nabla^*)(f_1^A)^2 + \beta^A(\nabla^*)(f_1^B)^2 + \alpha^{A-B}(\nabla^*) f_1^A f_1^B + \\
&\zeta^A |f_1^A|^2 f_1^A + \delta^A |f_1^B|^2 f_1^B + A^A |f_1^A|^2 f_1^B + B^A |f_1^B|^2 f_1^A + \\
&C^A (f_1^A)^*(f_1^B)^2 + D^A (f_1^B)^*(f_1^A)^2 + \cdots
\end{aligned} \tag{5.27}$$

and we don't explicitly write down terms that contain spatial derivatives of polar fields. We observe that all kind of possible linear, quadratic and cubic terms allowed by symmetry are present: we recall that under a rotation of angle ϕ each Fourier mode transforms as $f_k \xrightarrow{\phi} e^{ik\phi} f_k$. Thus our equation for f_1 can only consist of terms that transform as the first mode does; in other words the only allowed combination of polar fields are those which in total give a factor $e^{i\phi}$ if a rotation of ϕ is applied. To justify why terms like $\alpha^A(f_1^A)^2$ can be included, we have explicitly indicated the dependence of the coefficient on the complex operator ∇^*: this in fact transforms as $e^{-i\phi}$ and rotational symmetry is preserved.
The complete expressions for all coefficients are given in App. B.

5.3 Homogeneous polarized solution

Finding another solution for the Boltzmann equation (3.49) in addition to the trivial HIP one is not an easy (if possible) task. Nevertheless since the HIP is unstable and a transition towards order is observed, we ask ourselves whether the system reaches another homogeneous stationary state where our order parameter (i.e. f_1) is non zero. To tackle this problem we employ the hydrodynamic equations that we have

just derived for binary mixture to find a homogeneous ($\rho_A = const$, $\rho_B = const$) but polarized solution ($f_1^A = const \neq 0$, $f_1^B = const \neq 0$) that we will call HPP (Homogeneous Polarized Phase).

If we treat f_1^A and f_1^B as non zero constants we are left with Eq. (5.27) and with the corresponding equation for species B that we didn't write down. The equations for the densities of species A and B are of the form Eq. (5.4) and thus identically satisfied. Even if we have now reduced our problem to the solution of a system of algebraic equations, it is clear that a simple expression, where both polar field are different from zero, cannot be derived easily.
For this reason we first try to set to zero one of the two fields, say f_1^A, and find a non zero constant solution for f_1^B. What remains of the hydrodynamic equations is

$$\gamma^A f_1^B + \delta^A |f_1^B|^2 f_1^B = 0\,, \tag{5.28}$$

from Eq. (5.27) for species A, while from the corresponding equation for species B we obtain the condition

$$\mu^B f_1^B + \zeta^B |f_1^B|^2 f_1^B = 0\,. \tag{5.29}$$

Note that $\beta^{A(B)}(\nabla^*) = 0$ and $\alpha^{A(B)}(\nabla^*) = 0$, because we seek a uniform $\rho = const.$ solution. Since Eqs. (5.28) and (5.29) have to hold at the same time but the coefficients in front of each term are in general different from one another, there are only two possibilities: either $f_1^B = 0$ or

$$|f_1^B|^2 = -\frac{\gamma^A}{\delta^A} = -\frac{\mu^B}{\zeta^B}\,. \tag{5.30}$$

The solution $f_1^B = 0$ is consistent with our scaling ansatz: if $f_1^A \sim \mathcal{O}(\epsilon)$ and also $f_1^B \sim \mathcal{O}(\epsilon)$; setting $f_1^A = 0$ implies that the same must hold for f_1^B. Furthermore this means that $f_1^A \neq 0 \to f_1^B \neq 0$. In other words if species A is in a homogeneous-polarized state, also B must be in such a state. We will see that this is also in accordance with the numerical simulations.

The second solution provides instead the nontrivial condition

$$\frac{\gamma^A}{\delta^A} = \frac{\mu^B}{\zeta^B} < 0\,, \tag{5.31}$$

that corresponds to restricting the 4-dimensional parameter space to a 3-surface $\left[\frac{\gamma^A}{\delta^A} - \frac{\mu^B}{\zeta^B}\right](\rho_A, \rho_B, \sigma_A, \sigma_B) = 0$ with the additional requirement that $\frac{\gamma^A}{\delta^A}$ or equivalently $\frac{\mu^B}{\zeta^B}$, is negative. Even if the two conditions are satisfied on some 3-manifold of $\mathbb{R}^4$, fixing ρ_B and σ_B like we've done before means that the solution exists on a 1-curve that has measure 0 in the 2-dimensional phase space (σ_A, ρ_A). Moreover a

phase that exists only on a line in a two-dimensional space is not physically realizable: infinitely small perturbations would immediately drag the system towards a different critical point. We then claim that the only meaningful possibility is: $f_1^A = 0 \rightarrow f_1^B = 0$ that is equivalent to $f_1^A \neq 0 \rightarrow f_1^B \neq 0$. Numerical simulations are also in agreement with this last statement (see Sect. 6.2).

In principle it should be possible to construct other kinds of ansatz for a solution (for example a plane wave one), but introducing space dependence into an equation like Eq. (5.26) complicates things even more. Nevertheless, space dependent terms need to be retained if we wish to investigate the stability of a possible HPP solution against non homogeneous perturbation [32]. This is important as we will show in the next chapter that in our numerical simulations spatial patterns arise close to the transition line; however a complete analytical treatment is beyond the limits of this work as it would imply finding a general HPP solution (where both polar fields are non zero) and linearise the equations around this fixed point.

6 Numerical Analysis

Our study of the collective behaviour of an active binary mixture is based on the Boltzmann equation for the one-particle density function. The expansion in Fourier modes and the successive truncation of high order terms has allowed us to infer the phase diagram and to derive the hydrodynamic equations for the density and momentum field. However, all these techniques rely on assumptions that restrict their validity range. The numerical approach based on the SNAKE algorithm [47, 48] solves the equations of motion and thus has the great advantage of being applicable for all control parameter values (in our case density-noise) and of not relying on any fundamental assumptions but the ones implicit in the Boltzmann equation itself.
We will first verify our results from linear stability analysis and then concentrate on what happens at the transition order $\Leftrightarrow$ disorder. In particular, we will find that co-moving wave-like patterns form at the onset of order.
In the last section we present our data graphically (Sect. 6.2) and discuss the meaning of what we consider to be the main peculiarities of our system.

6.1 The SNAKE algorithm

In this section we will briefly outline the procedure conceived by F. Thüroff et al. in [47] to numerically solve the kinetic Boltzmann equation in real space

$$\partial_t f(\mathbf{r},\theta,t) + \mathbf{e}_\theta \cdot \nabla f(\mathbf{r},\theta,t) = I_d[f] + \rho_0 I_c[f]\,. \tag{6.1}$$

The *SNAKE* (Solving Numerical Active Kinetic Equations) algorithm is a discretization scheme for the Boltzmann equation in *real space* that makes use of a finite difference method: time is increased through tiny intervals τ so that the partial derivative with respect to time may be written (in the limit of small τ) in the following way

$$\partial_t f \to \frac{f(\mathbf{r},\theta,t+\tau) - f(\mathbf{r},\theta,t)}{\tau}\,, \tag{6.2}$$

while the gradient-proportional term in (3.5) can be thought as a directional derivative along $\mathbf{e}_\theta$

$$\mathbf{e}_\theta \cdot \nabla f(\mathbf{r},\theta,t) \to \frac{f(\mathbf{r},\theta,t) - f(\mathbf{r}-\tau\mathbf{e}_\theta,\theta,t)}{\tau}\,, \tag{6.3}$$

so that $f(\mathbf{r},\theta,t)$ cancels in the two derivatives. We then project the spatial domain on a two-dimensional square lattice of dimension L and constant ϵ.
The continuous angular interval $(-\pi,\pi]$ is then divided into a constant number M_θ of angular channels of size a

$$f(\mathbf{r},\theta,t) \to f(\mathbf{r}_i,\theta_k,t), \quad \mathbf{r}_i \in (1, L/\epsilon] \times (1, L/\epsilon], \quad k \in (1, 2\pi/a)\,. \tag{6.4}$$

The diffusion integral has the dimensionless form

$$I_d[f] = -f(\mathbf{r},\theta,t) + \int d\theta' f(\theta') \int d\eta P_0(\eta)\delta_{2\pi}(\theta'+\eta-\theta)\,, \tag{6.5}$$

that can be cast into the discrete version

$$-f(\mathbf{r}_i,\theta_k,t) + \sum_n \mathbf{P_0}_{(k,n)} f(\mathbf{r}_i,\theta_n,t) \tag{6.6}$$

or even in the more concise and useful notation

$$\sum_n \mathbf{D}_{k,n} f(\mathbf{r}_i,\theta_n,t)\,, \tag{6.7}$$

by defining the *diffusion operator*

$$\mathbf{D}_{k,n} := \mathbf{P_0}_{(k,n)} - \delta_{k,n}. \tag{6.8}$$

We now apply the discretization procedure to the collision term

$$\begin{aligned} I_c[f] = -f(\theta)\int d\phi R(|\theta-\phi|)f(\phi) + \int d\phi_1 d\phi_2 R(|\phi_1-\phi_2|)f(\phi_1)f(\phi_2) \\ \times \int d\eta P(\eta)\delta_{2\pi}(\bar{\theta}+\eta-\theta)\,, \end{aligned} \tag{6.9}$$

that becomes

$$-f(\mathbf{r}_i,\theta_k,t)\sum_m R(|\theta_k-\theta_m|)f(\mathbf{r}_i,\theta_m,t) + \sum_{l,m}\mathbf{P}_{k,m,l}R(|\theta_l-\theta_m|)f(\mathbf{r}_i,\theta_l,t)f(\mathbf{r}_i,\theta_m,t) \tag{6.10}$$

or

$$\sum_{l,m}\mathbf{C}_{k,l,m}f(\mathbf{r}_i,\theta_l,t)f(\mathbf{r}_i,\theta_m,t)\,, \tag{6.11}$$

with the following definition of the *collision operator*

$$\mathbf{C}_{k,l,m} = \mathbf{P}_{k,l,m}R(|\theta_l-\theta_m|) - \delta_{k,l}R(|\theta_k-\theta_m|)\,. \tag{6.12}$$

The last term $f(\mathbf{r}-\tau\mathbf{e}_\theta,\theta,t)$ which accounts for convection, can be rewritten as

$$\sum_l \mathbf{T}_{k,l}(\tau)f(\mathbf{r}_i,\theta_l,t)\,, \tag{6.13}$$

with the definition of the *convection operator* that can be understood looking at Fig. 15. The matrix element $\mathbf{T}_{k,l}$ gives the fraction of particles that in the time interval $(t,t+\tau)$ moved from lattice site l to lattice site k and it can be derived with simple

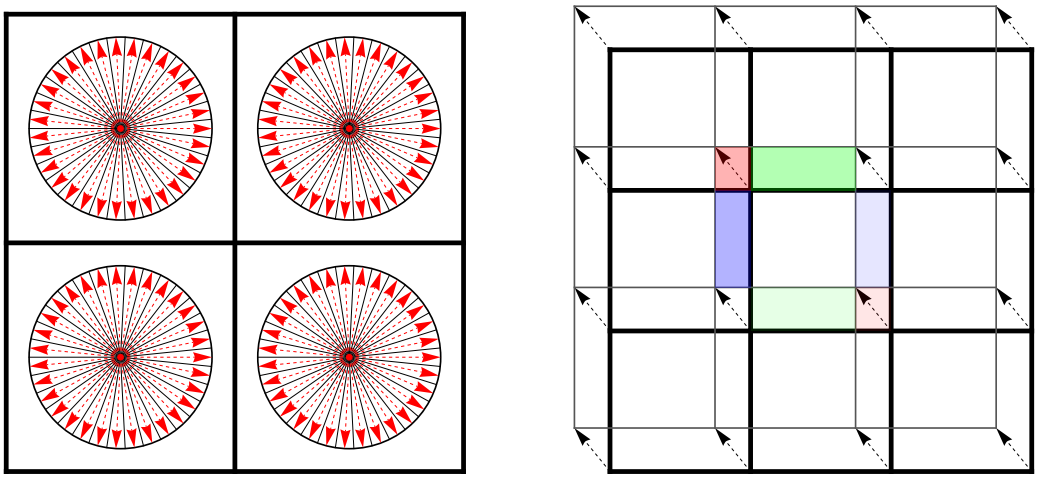

Figure 15: *Left:* Illustration of the lattice structure. Each space element is represented by a black square of side length ϵ. Appended to each lattice site is a constant number of angular slices (M_θ slices; indicated by the circles and red arrows). The k^{th} angular slice at lattice site (α, β) stores the value of $f(\{x_\alpha, y_\beta\}, \theta_k, t)$. *Right:* Illustration of the convection step. The length of the dashed arrows indicates the length of the time step τ, the direction of the dashed arrows indicates the angular channel being streamed. The colored regions indicate the fraction of $f(\{x_\alpha, y_\beta\}, \theta_k, t)$ converted to neighboring lattice sites [darker colors: convection out of (α, β); lighter colors: convection into (α, β); cf. Eq. (6.13)]. Note that we have to choose $\tau/\epsilon \ll 1$ to make the number of collisions between particles situated at different lattice sites at time t small (otherwise a local evaluation of the collision processes is not justified).

Figure courtesy of F. Thüroff and C. A. Weber.

geometrical considerations. One necessary condition is that $\tau \ll \epsilon$, so that we can fulfil the requirement from the Boltzmann equation that collisions are local. This has to be taken in consideration when specific parameters for the simulations are chosen.

We can now collect all discretised terms of the equation to obtain the update rule

$$\begin{aligned} f(\mathbf{r}_i, \theta_k, t+\tau) = &\sum_l \mathbf{T}_{k,l}(\tau) f(\mathbf{r}_i, \theta_l, t) + \tau \sum_n \mathbf{D}_{k,n} f(\mathbf{r}_i, \theta_n, t) \\ &+ \hat{\rho}\, \tau \sum_{l,m} \mathbf{C}_{k,l,m} f(\mathbf{r}_i, \theta_l, t) f(\mathbf{r}_i, \theta_m, t) \end{aligned} \tag{6.14}$$

that corresponds to an Euler forward algorithm where the updated distribution function at time $t + \tau$ is calculated from the know distribution at time t.

F. Thüroff and C. A. Weber constructed the Boltzmann equation solver [47, 49] for a single species of particles: in order to numerically simulate our system we

have extended and modified it including another self-propelled particle species. Therefore instead of having one single density distribution function f, we now simulate the temporal evolution of two density distributions (f^A and f^B) by means of two convection, two diffusion and two collision operators independent from one another. Additionally, to account for inter-species collisions $\Leftrightarrow$ we introduce a new nonlinear term in the discretization scheme. The algorithm updates the distribution functions for species A and B, f^A and f^B respectively, at the same time by applying the following rule

$$f^A(\mathbf{r}_i,\theta_k,t+\tau) = \sum_l \mathbf{T}_{k,l}(\tau) f^A(\mathbf{r}_i,\theta_l,t) + \tau \sum_n \mathbf{D}^A_{k,n} f^A(\mathbf{r}_i,\theta_n,t)$$
$$+ \tau \sum_{l,m} \left[\hat{\rho}_A \mathbf{C}^A_{k,l,m} f^A(\mathbf{r}_i,\theta_l,t) f^A(\mathbf{r}_i,\theta_m,t) + \hat{\rho}_B \mathbf{C}^{A-B}_{k,l,m} f^A(\mathbf{r}_i,\theta_l,t) f^B(\mathbf{r}_i,\theta_m,t) \right] \tag{6.15}$$

$$f^B(\mathbf{r}_i,\theta_k,t+\tau) = \sum_l \mathbf{T}_{k,l}(\tau) f^B(\mathbf{r}_i,\theta_l,t) + \tau \sum_n \mathbf{D}^B_{k,n} f^B(\mathbf{r}_i,\theta_n,t)$$
$$+ \tau \sum_{l,m} \left[\hat{\rho}_B \mathbf{C}^B_{k,l,m} f^B(\mathbf{r}_i,\theta_l,t) f^B(\mathbf{r}_i,\theta_m,t) + \hat{\rho}_A \mathbf{C}^{A-B}_{k,l,m} f^B(\mathbf{r}_i,\theta_l,t) f^A(\mathbf{r}_i,\theta_m,t) \right] \tag{6.16}$$

where the new letter indices indicate that the operator includes the parameters for species A or for species B. The convection operator only depends on the time-step τ, thus it is the same for both. Regarding the "new" factors in front of the mutual-collisions operator ($\hat{\rho}_B$ for species A and $\hat{\rho}_A$ for species B), they are a result of the rescaling choice $f_A \to f_A/\rho_A$ and $f_B \to f_B/\rho_B$.

6.2 Numerical results

In this final section of the thesis we want to present our numerical results obtained from numerical simulations carried out via the *SNAKE algorithm*, a *C++* implementation of the update rules Eqs. (6.15) and (6.16). The program takes as input the parameters that define the model: density and noise for both species as well as inter-species noise. To compare numerical results to analytical ones (mainly linear stability), we have set the self-diffusion noise equal to the collision noise and σ_{A-B} equal to the average of the two (Eqs. (3.44)-(3.46)). Our simulations were performed on a rather small 10×10 lattice with spacing $\epsilon = 0.5$, time step $\tau = 0.05$ (note $\tau \ll \epsilon$) and with a total number of angular channels $M_\theta = 28$. The total duration of our simulations was $T \approx 40000$. A random density distribution $f(\mathbf{r}_{i,j},\theta_k,t=0)$ both

over the lattice and over the angular channels was employed as initial configuration of the system. A few snapshots of a bigger system are shown in Fig. 16, 19, 20, 21 to better display wave patterns and the evolution of heterogeneities over time.

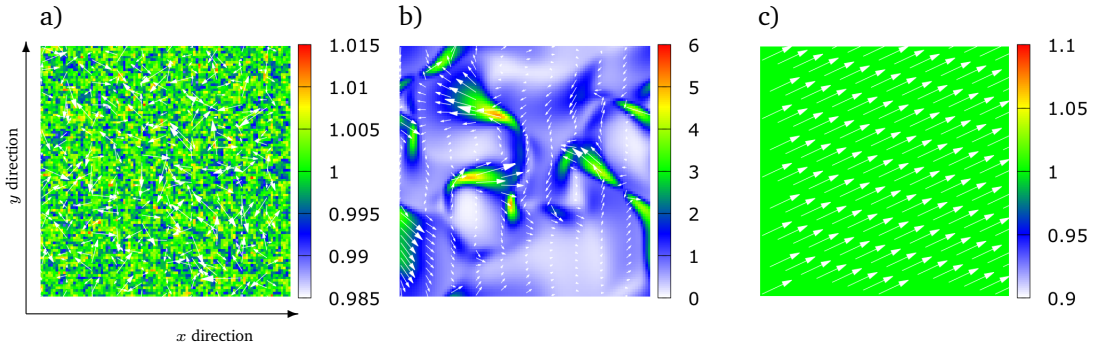

Figure 16: *From left to right:* snapshots of a 100×100 grid evolving in time from a random initial configuration towards homogeneous polar order. In a) we plot the two axes indicating the two orthogonal directions on our lattice. The *color* indicates the density at each point in space, changing from green (lowest) to white (highest). Each arrow indicates the direction of motion at that point on the lattice: they are rescaled for better visualization.

To plot the nonequilibrium phase diagram for the system we calculate the average momentum over the whole lattice when the system reaches its relaxed stationary state and distinguish between polar ordered and disordered phase.
The first thing that comes to our attention is that the two plots for the phase diagram Fig. 17-18 are completely identical: this means that the two species have the same *average* behaviour throughout the parameter space. By "average behaviour" we mean that even if the phase is clearly the same at the same point on the lattice, locally the two species show differences in momentum and density. This is consistent with our linear analysis that cannot yield anything but a single phase diagram describing the system as a whole. Looking for example at Fig. 17 a) we realize that, except for a few "anomalous" ones, blue dots (HPP) are below the black transition line while orange points (HIP) are above it, thus mostly agreeing with Fig. 10 a).

In Fig. 18 we displayed the phase diagram for $\sigma_B = 0.5$, while $\rho_B = 0.4$ as before. Also in this case the two species share the same phase diagram, once again confirming their entwined evolution, as our linear stability had suggested. Since we have increased the noise of species B, we would expect the disordered state (*orange*) to occupy the region above the concavity of the transition curve, as shown in Fig. 10 d). This is what our numerical plots also reveal, except for a few blue points that occupy the region close to the transition line. When we compare linear stability plots to Fig. 18 we can recognize the same kind of "anomaly" as in Fig. 17, i.e. the system drifts towards order too early in parameter space. With "too early" we mean that

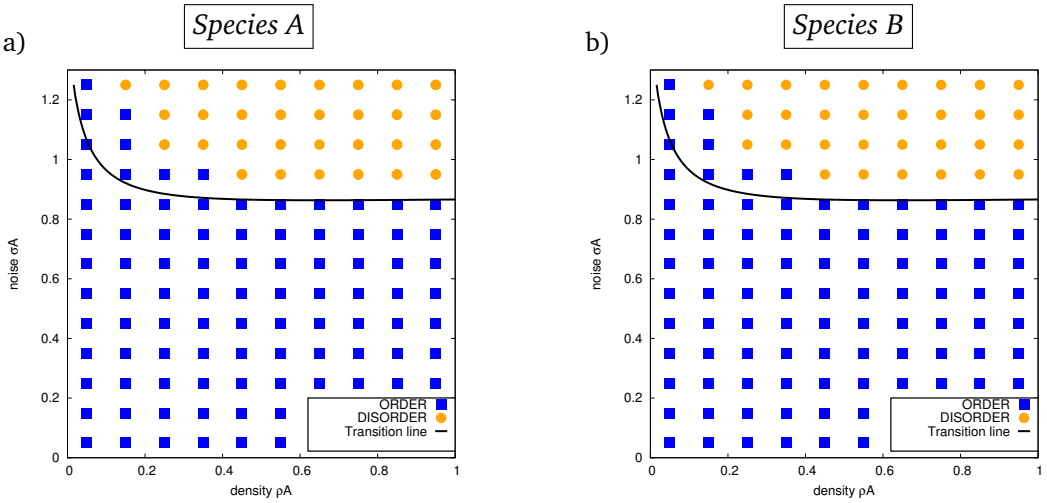

Figure 17: *Parameters*: $\rho_B = 0.4$, $\sigma_B = 0.5$.
Right: phase diagram for species A. *Left*: phase diagram for species B.
Blue: ordered region. *Orange:* disordered region.
It is evident that the two species share exactly the same phase diagram, confirming our stability analysis.

for example setting the noise to a constant $\sigma_A = 0.35$ in Fig. 18 and increasing the density starting from the y axis, we encounter order before effectively crossing the transition line. The same holds for the phase diagram of Fig. 17 but for higher noise and in the "reversed direction".

Trying to justify this discrepancy, we recall that although the transition disorder $\Leftrightarrow$ order was originally thought to be continuous [54], it was more recently pointed out by Chaté, Gregoire *et al.* [10, 22, 23] that in the limit of big system size the transition seems instead to be discontinuous, with formation of heterogeneities.

The debate was further enriched by numerical simulations of mean-field theories for the Vicsek model that were able to numerically find soliton-like waves in the limit of high speed: these are able to change the nature of the transition from continuous to discontinuous [25]. The fact that the transition disorder-order may exhibit hysteresis suggests that different initial conditions might shed more light on the mentioned anomalies. Assuming that when the simulations are started the total average momentum is already above the attractive region of our HIP fixed point, this causes the system to evolve towards an HPP stationary state despite being in the stability region of the isotropic critical point. Hysteresis may even emerge in the transition between different possible homogeneous states: this interesting hypothesis relates to the question we asked when deriving the hydrodynamic equations, i.e. if

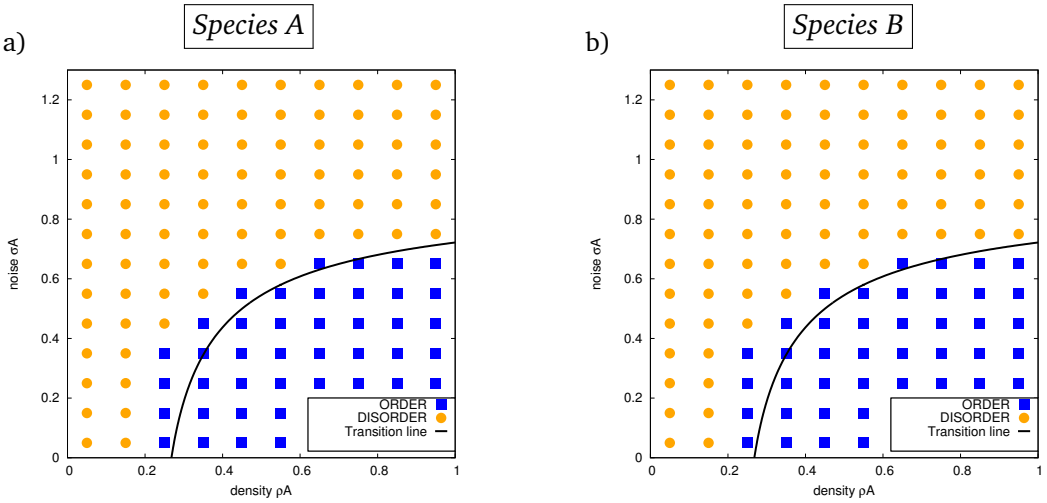

Figure 18: *Parameters*: $\rho_B = 0.4$, $\sigma_B = 0.9$.
Right: phase diagram for species A. *Left*: phase diagram for species B.
Blue: ordered region. *Orange:* disordered region.
The two species share exactly the same phase diagram, confirming our stability analysis.

more than one nontrivial homogeneously ordered solutions exist in our system.

In contrast to a number of previous studies on single species systems [10, 25, 47], our ordered phase only exhibits homogeneous steady states. We speculate that this might be due to the small system sizes considered here [10], nevertheless we expect (and observe for larger systems) density waves and possibly cluster-lane patterns [47] to form in the vicinity of the binary-mixture transition line. In Fig. 19 the system is organizing into a stripe-structured pattern. The 64×64 lattice employed here seems to be big enough for heterogeneities to build up and eventually converge into a density wave. What usually happens is that two or more regions of high density group together and start moving in one direction on a low-density isotropic substrate. However, we stress the fact that there is no a priori reason why density waves should be observed in a binary mixture if not for similarity with the single species case.

The snapshot of Fig. 20 is taken for a system slightly above the transition line: $\rho_A = 0.15$, $\sigma_A = 1.05$ and $\sigma_B = 0.5$. It shows how even in the situation where spatial patterns arise, the two species share the same behaviour: the two density waves propagate in a common direction, with equal speeds. However if we "cut" the plane along the diagonal and plot the profile of the waves as we move from the lower left corner to the upper right one we find two distinct shapes. This effect might be due to our choice to implement a model with equal speeds for the two species, yet it is not

guaranteed that this is the only reason why no de-mixing is observed. For example phase separation was shown to occur in the case of differently shaped particles [58] and/or in the case of variable speed [33]. Using the same data as for Fig. 21 we

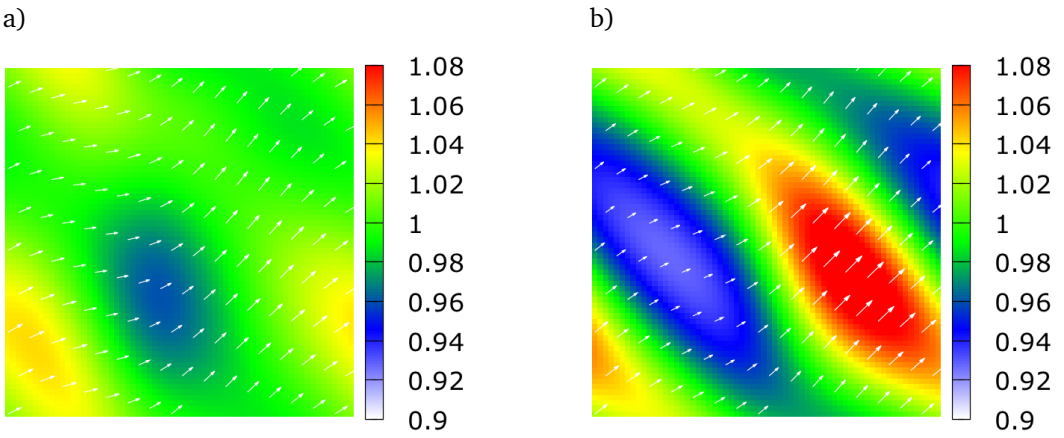

Figure 19: *Left to right:* Two snapshots of the wave-forming process at two different times $t_{right} > t_{left}$. We can see that two regions of higher density (yellow) are separated by a low density region (blue) that will become the trough of the wave. The two yellow-red regions (here the density is the highest) shown on the left eventually become one single peak whose lateral extent is the whole lattice diagonal.

have plotted in Fig. 22 the density profiles of the two waves at the same time. From this plot the front rear asymmetry [6, 25, 47] is clear: the density jump at the front is much steeper than the one at the back, the difference becoming more and more evident as we increase the density further in the ordered region (see Fig. 4 a) of Ref. [47]). Furthermore the density difference in the two species is reflected in the more pronounced peak for species B ($\rho_A = 0.15 < \rho_B = 0.4$).

The phase diagrams in Fig. 17 and Fig. 18 mostly confirm our stability analysis, except for parameters close to the transition line: as already mentioned, hysteresis effects could explain why this inconsistency takes place. However a bigger lattice, a higher parameter discretization (density and noise are increased by 0.1 between each simulation) and, most importantly, implementations with different initial conditions are needed to examine the nature of this phenomenon. Nevertheless we can firmly state that the trend derived from linear stability is the same as found in numerical simulations. In particular the transition line is undoubtedly the one shown in Fig 10 for the two noise values chosen for our numerical investigations; the emergence of a density threshold for $\sigma_B = 0.9 > \sigma_{crit}$ and the possibility, for $\sigma_B = 0.5 < \sigma_{crit}$ of entering the disordered region by increasing the density (see Fig. 17), both distinctive characteristics of an active binary mixture, are confirmed. Besides validating our

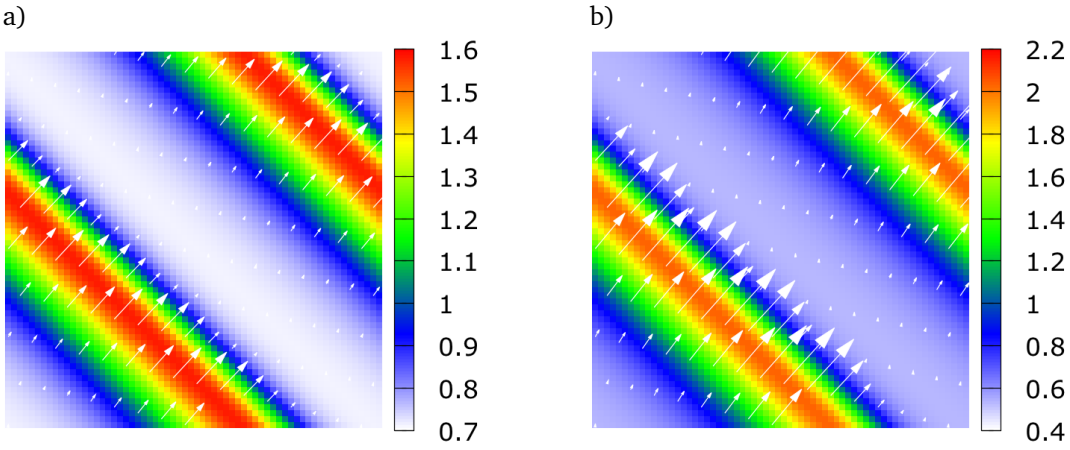

Figure 20: Snapshot of a density wave propagating along diagonal of the lattice: on the *right* an example of wave for species A and on the *left* one for species B. As anticipated both species move in the same direction with the same speed. The typical front-rear asymmetry, characteristic feature of this density waves is also present. Moreover a difference in the profile of the wave can be seen between a) and b).

stability analysis, SNAKE has given us more insight about what kind of solutions are to be found inside the order region: "coupled" wave-like patterns form in the mixture at the onset of instabilities, where by "coupled" we mean that A-particles and B-particles move in the same direction thus avoiding any de-mixing effect in the system. We then infer that differences in macroscopic density and stochastic noise are not sufficient to yield phase-separation between the two species. Other studies suggest that differentiating particles by their speed and/or their shape may instead induce separate segregation [33, 58]. Nevertheless the main feature of this kind of density waves, namely the front-rear asymmetry is retained: notice that this property depends on the overall density of the species (see Fig. 22) and it is more pronounced the bigger the density [32, 47, 48]. No other variety of spatial patterns (like for example the cluster lanes of Ref. [47]) was found in our simulations: still the region close to the onset of order deserves by itself a much deeper analysis, given the abundance of interesting phenomena reported in particle simulations [1, 25, 33, 58].

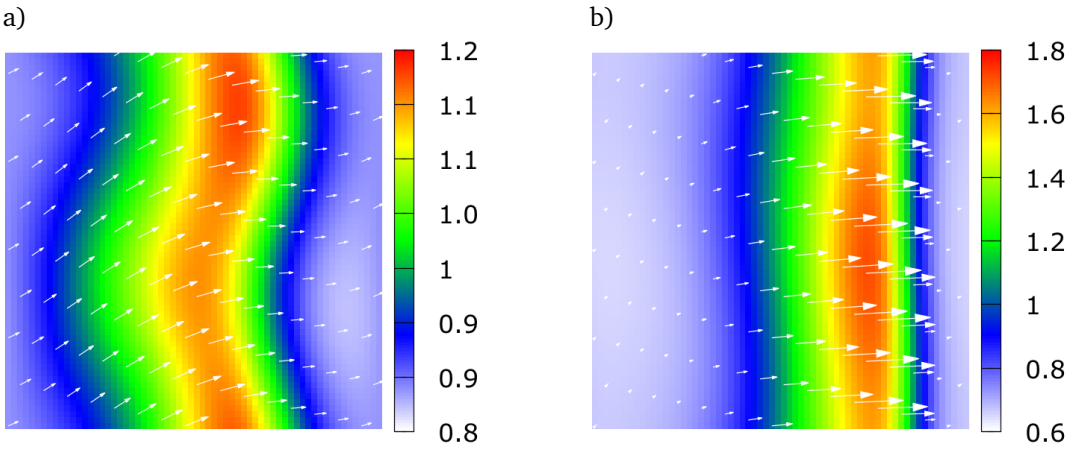

Figure 21: Structure of a wave propagating along the x-axis: from the coalescence of two vertically separate high density regions a belly-shaped pattern is formed. Eventually this vertical asymmetry disappears while the typical front-rear asymmetric wave profile is developed.

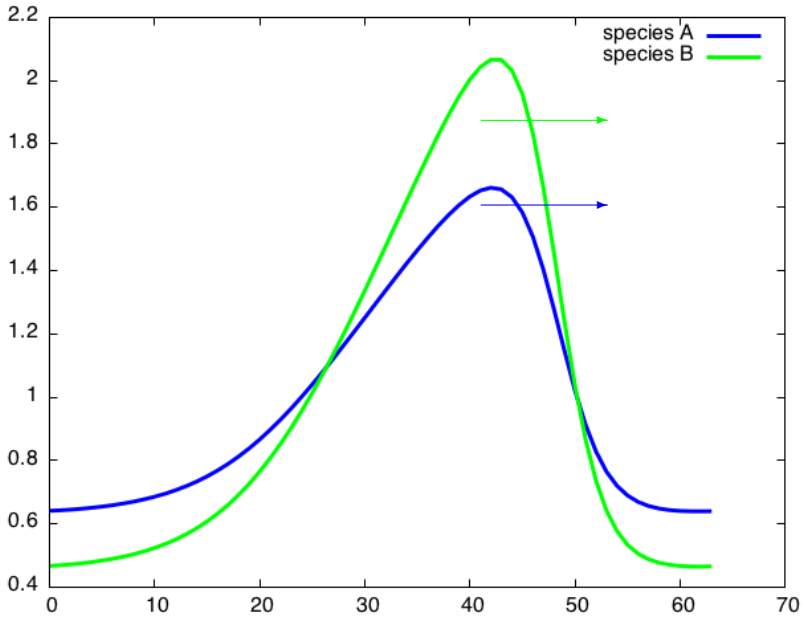

Figure 22: The density profiles for a wave of species A (*blue*) and of species B (green) are drawn. The two patterns have the same direction (indicated by the two arrows) and almost fully overlap (both species have the same speed) but not the same shape (densities are different).

Conclusions

Diversity in active systems such as bacterial populations [4], polymer suspensions [18], as well as in fish schools [33] or swarms of insects [40] is a fundamental and intrinsic property of many out-of-equilibrium biophysical systems.
The main purpose of the thesis was to approach the study of heterogeneous active systems. In the spirit that characterises physical sciences, we have simplified our problem as much as possible first looking at binary mixtures of self-propelled point-like particles moving in a non-conservative fashion on a plane. The two species differ from one another in density and stochastic noise. A kinetic Boltzmann approach was employed for this study: all our work is therefore based on the hypothesis of molecular chaos and pairwise interactions. Furthermore, our model only considers a polar alignment rule both for intra-species and inter-species collisions.

As a first step into the world of binary self-propelled particles we devised the equations for the two polar-fields (first Fourier mode) and for the densities. We then applied linear stability analysis close to the homogeneous and isotropic phase (HIP) of such equations, motivating our choice for the eigenvalue-eigenvector pair that correctly accounts for polar alignment. This gave us a whole new picture of what really happens when two distinct active populations are mixed together: the non-equilibrium phase diagram shows that mixing two disordered species may in general give rise to an ordered mixture and confirms the intuition that introducing additional polar collisions between the two species does not suppress order.
In addition to that we pointed out the possibility of a re-entrant phase transition for noise values close to criticality and the emergence at higher noise values of a disorder $\Rightarrow$ order transition-threshold in the density. If instead the noise of the "control" species is chosen below the critical value, an order $\Rightarrow$ disorder transition takes place by increasing the density of the other. The stability of the homogeneous-polarized phase (HPP) was also tested against plane wave perturbations: the behaviour remains unchanged and the dispersion relation for parameters above criticality suggests that the phase transition is dominated by a homogeneously growing order.

Motivated by the possibility of calculating a homogeneous but polarized solution analytically from our equations, we successfully derived the set of hydrodynamic equations for the density and polar fields for each species, adopting the procedure described in [6]. Despite the quite unhandy coefficients for a few terms, we were able to confirm one of the results obtained from linear stability, supported also by successive numerical simulations: if the momentum field of species A vanishes, so has to be for species B.

In the last part of the thesis our analytical results were numerically tested employing the SNAKE algorithm [49], appropriately modified to handle two distinct

species interacting with each other. The great advantage of numerical approaches, namely to explore parameter regions for which linear stability is not conclusive or not applicable, was exploited to investigate which kind of patterns arise at the onset of order and deep inside the instability region of the HIP. This numerical tool helped us in the process of understanding how our mixture behaves: possibly due to our choice of differentiating particles according to their density or to their noise, we always observed deeply entwined patterns. The same type of density waves as for example in [47] were discovered close to the transition line both for species A and B (for a system large enough). The wave profile is different but the direction, speed and region of existence are the same. Consequently, we end up with equal numerical phase diagrams where no de-mixing behaviour is observed. We postulate that if spatial properties like shape, speed or even curvature were the characterizing differences between the two populations in the mixture (instead of noise for example), we would detect clustering, phase separation and other separate-grouping behaviour [1, 33, 58].

Other recent findings in Brownian dynamics simulations e.g. in [19], seem to confirm the rich variety of different possible phenomena happening in heterogeneous populations. Excited for what is still to come, we suggest that the Boltzmann approach may give promising results also in variable-speed mixtures, in particles with different chirality (curvature) or in systems with broken particle-shape symmetry.

In summary our work has shown that the behaviour of two different species changes significantly when they are mixed together with an additional polar alignment rule. This is revealed by the non-equilibrium phase diagram of a binary mixture, derived both analytically and numerically. In addition to disorder and homogeneous polar order, we found density-wave patterns close to the transition line, both in species A and in species B, but no de-mixing behaviour was observed: we suggest that a different characterization of the two species for their intrinsic properties might instead lead to phase separation.

Appendices

A Fourier transform of the collision integral

The gain term of the collision integral is transformed in the following way for a *polar* collision rule:

$$
\begin{aligned}
I^G_{c,k} &= \int d\theta e^{ik\theta} \int_{-\pi}^{\pi} d\theta_1 d\theta_2 R(\theta_2-\theta_1) f(\theta_1) f(\theta_2) \int_{-\infty}^{\infty} d\eta P(\eta) \\
&\times \delta_{2\pi}(\Psi(\theta_1,\theta_2)+\eta-\theta) \\
&= \frac{1}{(2\pi)^2} \sum_{p,q} \hat{f}_p \hat{f}_q \int d\theta e^{ik\theta} \int d\theta_1 e^{-ip\theta_1} \int d\theta_2 e^{-iq\theta_2} R(\theta_2-\theta_1) \int_{-\infty}^{\infty} d\eta P(\eta) \\
&\times \delta_{2\pi}((\theta_1+\theta_2)/2+\eta-\theta) \\
&= \frac{1}{(2\pi)^2} \sum_{p,q} \hat{f}_p \hat{f}_q \int d\theta_1 e^{-ip\theta_1} \int d\Delta e^{-iq(\Delta+\theta_1)} R(\Delta) \int_{-\infty}^{\infty} d\eta P(\eta) \\
&\times \int d\theta e^{ik\theta} \delta_{2\pi}(\theta_1+\Delta/2+\eta-\theta) \\
&= \frac{1}{(2\pi)^2} \sum_{p,q} \hat{f}_p \hat{f}_q \int d\Delta R(\Delta) \int_{-\infty}^{\infty} d\eta P(\eta) \\
&\times \int d\theta_1 e^{-ip\theta_1} e^{-iq(\theta_1+\Delta)} e^{ik(\theta_1+\Delta/2+\eta)} \\
&= \frac{1}{(2\pi)^2} \underbrace{\int d\theta_1 e^{i(k-q-p)\theta_1}}_{=2\pi\delta_{k-q,p}} \sum_{p,q} \hat{f}_p \hat{f}_q \int d\Delta R(\Delta) e^{i(k/2-q)\Delta} \\
&\times \underbrace{\int_{-\infty}^{\infty} d\eta P(\eta) e^{ik\eta}}_{=:P_k} \\
&= \frac{1}{2\pi} \sum_{q} \hat{f}_q \hat{f}_{k-q} P_k \int_{-\pi/2}^{\pi/2} d\Delta\, R(\Delta) \cos((q-k/2)\Delta)\,.
\end{aligned}
$$

In the case of an *antipolar* collision rule:

$$\Psi(\theta_1,\theta_2)=\begin{pmatrix}\Psi_1(\theta_1,\theta_2)\\ \Psi_2(\theta_1,\theta_2)\end{pmatrix}=\begin{cases}\begin{pmatrix}(\theta_1+\theta_2)/2+\pi/2\\ (\theta_1+\theta_2)/2-\pi/2\end{pmatrix} & \text{if} \quad \pi/2<|\theta_2-\theta_1|<\pi\\ \\ \begin{pmatrix}\theta_1\\ \theta_2\end{pmatrix} & \text{else}\,.\end{cases} \tag{A.1}$$

So that Eq. (3.28) for the gain term (the loss one remains the same) can be rewritten separating the two contributions Ψ_1 and Ψ_2

$$\begin{aligned}\int d\theta\, e^{ik\theta} I_c^{G,antipolar}[f] = \int d\theta e^{ik\theta}\int_{-\pi}^{\pi} d\theta_1 d\theta_2 R(\theta_1,\theta_2) f(\theta_1) f(\theta_2)\int_{-\infty}^{\infty} d\eta P(\eta)\\ \times\left(\frac{1}{2}\delta_{2\pi}(\Psi_1(\theta_1,\theta_2)+\eta-\theta)+\frac{1}{2}\delta_{2\pi}(\Psi_2(\theta_1,\theta_2)+\eta-\theta)\right),\end{aligned} \tag{A.2}$$

that is similar to the polar case, except for the additional factors $\pm\pi/2$ that shift the complex exponential, resulting in

$$\begin{aligned}I_{c,k}^{G,antipolar} &= \frac{1}{(2\pi)^2}\sum_{p,q}\hat{f}_p\hat{f}_q\int d\Delta R(\Delta)\int_{-\infty}^{\infty} d\eta P(\eta)\\ &\times\int d\theta_1 e^{-ip\theta_1}e^{-iq(\theta_1+\Delta)}\frac{1}{2}(\underbrace{e^{ik(\theta_1+\Delta/2+\eta+\pi/2)}+e^{ik(\theta_1+\Delta/2+\eta-\pi/2)}}_{=e^{ik(\theta_1+\Delta/2+\eta)}(2\cos(k\pi/2))}\\ &= \frac{1}{2\pi}\sum_q \hat{f}_q\hat{f}_{k-q}\,P_k\cos(k\pi/2)\int_{\pi/2}^{3/2\pi} d\Delta\, R(\Delta)\cos((q-k/2)\Delta)\,.\end{aligned}$$

Adding the unchanged "loss" contribution we obtain the final expression of the Fourier transform of the collision integral for an *antipolar* collision rule

$$I_{c,k}^{antipolar}=\frac{1}{2\pi}\sum_q \hat{f}_q\hat{f}_{k-q}\int_{\pi/2}^{3/2\pi} d\Delta\, R(\Delta)\,(P_k\cos(k\pi/2)\cos((q-k/2)\Delta)-\cos(q\Delta)) \tag{A.3}$$

or as before

$$\sum_q I_{q,k}^{antipolar}\hat{f}_q\hat{f}_{k-q} \tag{A.4}$$

with

$$I_{q,k}^{antipolar}=\int_{\pi/2}^{3/2\pi}\frac{d\Delta}{2\pi}\,R(\Delta)\,(P_k\cos(k\pi/2)\cos((q-k/2)\Delta)-\cos(q\Delta)) \tag{A.5}$$

The case of *nematic* collisions is a combination of the two preceding rules

$$\Psi(\theta_1,\theta_2)=\begin{pmatrix}\Psi_1(\theta_1,\theta_2)\\ \Psi_2(\theta_1,\theta_2)\end{pmatrix}=\begin{cases}\begin{pmatrix}(\theta_1+\theta_2)/2\\ (\theta_1+\theta_2)/2\end{pmatrix} & \text{if} \quad |\theta_2-\theta_1|<\pi/2\\ \begin{pmatrix}(\theta_1+\theta_2)/2+\pi/2\\ (\theta_1+\theta_2)/2-\pi/2\end{pmatrix} & \text{if} \quad \pi/2<|\theta_2-\theta_1|<\pi\\ \begin{pmatrix}\theta_1\\ \theta_2\end{pmatrix} & \text{else}\,.\end{cases} \tag{A.6}$$

The coefficients $I_{q,k}$ also have two contributions

$$\begin{aligned}I_{q,k}^{\text{nematic}}=&\underbrace{\int_{-\pi/2}^{\pi/2}\frac{d\Delta}{2\pi}\,R(\Delta)\cos((q-k/2)\Delta)}_{\text{polar}}\\ &+\underbrace{\int_{\pi/2}^{3/2\pi}\frac{d\Delta}{2\pi}\,R(\Delta)\left(P_k\cos(k\pi/2)\cos((q-k/2)\Delta)-\cos(q\Delta)\right)}_{\text{antipolar}}\end{aligned} \tag{A.7}$$

B Coefficients for the Hydrodynamic Equations

$$\mu^A = P^A_{0,1} - 1 + (I^{A-A}_{0,1} + I^{A-A}_{1,1})\rho_A + I^{A-B}_{1,1}\rho_B$$

$$\gamma^A = I^{A-B}_{0,1}\rho_A$$

$$\alpha^A = \frac{1}{2}\nabla^*\left(\frac{I^{A-A}_{1,2}\nu^A}{1-\nu^A\nu^B(I^{AB}_{0,2})^2\rho_A\rho_B}\right)$$

$$\beta^A = -\frac{1}{2}\nabla^*\left(\frac{I^{A-B}_{0,2}(\nu^A)^3}{1-\nu^A\nu^B(I^{AB}_{0,2})^2\rho_A\rho_B}\right)$$

$$\alpha^{A-B} = \frac{1}{2}\nabla^*\left(\frac{I^{A-B}_{1,2}\nu_A}{1-\nu^A\nu^B(I^{AB}_{0,2})^2\rho_A\rho_B}\right) - \frac{1}{2}\nabla^*\left(\frac{I^{A-B}_{0,2}(\nu^A)^3\rho_A I^{B-A}_{1,2}}{1-\nu^A\nu^B(I^{AB}_{0,2})^2\rho_A\rho_B}\right)$$

$$\zeta^A = -(I^{A-A}_{-1,1} + I^{A-A}_{2,1})\frac{\nu_A I^{A-A}_{1,2}}{1-\nu^A\nu^B(I^{AB}_{0,2})^2\rho_A\rho_B} - \frac{I^{A-B}_{-1,1}I^{A-B}_{0,2}I^{A-A}_{1,2}\nu^A\nu^B\rho_B}{1-\nu^A\nu^B(I^{AB}_{0,2})^2\rho_A\rho_B}$$

$$\delta^A = \frac{I^{A-B}_{2,1}I^{A-B}_{0,2}I^{B-B}_{1,2}\rho_A(\nu^A)^2}{1-\nu^A\nu^B(I^{AB}_{0,2})^2\rho_A\rho_B}$$

$$A^A = \frac{I^{A-B}_{-1,1}I^{B-A}_{0,2}I^{A-B}_{1,2}\nu^A\nu^B\rho_B}{1-\nu^A\nu^B(I^{AB}_{0,2})^2\rho_A\rho_B} - \frac{I^{AB}_{-1,1}I^{BA}_{0,2}I^{AB}_{0,2}I^{BA}_{1,2}(\nu^A)^2\nu^B\rho_A}{1-\nu^A\nu^B(I^{AB}_{0,2})^2\rho_A\rho_B}$$

$$- \frac{(I^{A-A}_{-1,1} + I^{A-A}_{2,1})I^{AB}_{1,2}}{1-\nu^A\nu^B(I^{AB}_{0,2})^2\rho_A\rho_B} - \frac{(I^{A-A}_{-1,1} + I^{A-A}_{2,1})I^{BA}_{1,2}\nu^A}{1-\nu^A\nu^B(I^{AB}_{0,2})^2\rho_A\rho_B}$$

$$B^A = -\frac{I^{AB}_{2,1}I^{AB}_{1,2}\nu^A}{1-\nu^A\nu^B(I^{AB}_{0,2})^2\rho_A\rho_B} + \frac{I^{AB}_{2,1}I^{AB}_{0,2}I^{BA}_{1,2}(\nu^A)^2\rho_A}{1-\nu^A\nu^B(I^{AB}_{0,2})^2\rho_A\rho_B}$$

$$C^A = -\frac{I^{AB}_{-1,1}I^{BA}_{0,2}I^{AB}_{0,2}I^{BB}_{1,2}(\nu^A)^2\nu^B\rho_A\rho_B}{1-\nu^A\nu^B(I^{AB}_{0,2})^2\rho_A\rho_B} + \frac{(I^{A-A}_{-1,1} + I^{A-A}_{2,1})I^{AB}_{0,2}I^{BB}_{1,2}(\nu^A)^2\rho_A}{1-\nu^A\nu^B(I^{AB}_{0,2})^2\rho_A\rho_B}$$

$$D^A = -\frac{I^{AB}_{2,1}I^{AA}_{1,2}\nu^A}{1-\nu^A\nu^B(I^{AB}_{0,2})^2\rho_A\rho_B}$$

Danksagung-Ringraziamenti

Ich möchte mich hiermit ganz herzlich bei Prof. Frey bedanken, für die Möglichkeit meine Masterarbeit mit Ihm und seiner Gruppe zu schreiben. Die inspirierende Atmosphäre und freundliche Leute mit den ich reden und diskutieren konnte, haben erheblich zum Erfolg meiner Arbeit beigesteuert.
Insbensondere wäre dieses Projekt ohne der Geduld und konstanten Unterstützung meiner beiden PhD-Betreuer, Jonas und Lorenz, nicht zu Leben gekommen sein.

Ringrazio il mio relatore Prof. Orlandini per le correzioni e il supporto durante il periodo di Tesi.

Un enorme "grazie" va alla mia famiglia: alle mie due sorelle Laura e Sofia ed in particolare a Mamma e Papà che mi hanno sempre sostenuto, non solo economicamente, e che credono così tanto in me.
Grazie alle mie due Nonne che sarebbero incredibilmente orgogliose di me, a mio zio Fausto, a mia zia Nadia ed alle mie cugine Giulia e Margherita.
Non sarei mai arrivato fino a questo punto, né avrei mai pensato di affrontare un Dottorato, se al mio fianco non ci fosse sempre stato il mio fan numero uno, il mio "fratello maggiore": mio zio Roberto.
Vorrei inoltre ringraziare tutti i miei amici sia di Padova che di Monaco per tutte le avventure passate assieme; particolare menzione per la banda di pirati BrochenOll a cui va un grosso "Arrrrr"!!

Un ringraziamento infine ad una persona importante che viene dall'altro capo del mondo e che sta rendendo questi momenti ancor più speciali: Lorraine.

A tutti voi e a tutti quelli che mi vogliono bene, va il mio riconoscente "grazie".

References

[1] G. Ariel, O. Rimer, E. Ben-Jacob, *Order-Disorder Phase Transition in Heterogeneous Populations of Self-propelled Particles*, Journal of Statistical Physics, Volume 158, Issue 3, pp.579-588, DOI:10.1007/s10955-014-1095-7.

[2] M. Ballerini, N. Cabibbo, R. Candelier, A. Cavagna, E. Cisbani, I. Giardina, A. Orlandi, G. Parisi, A. Procaccini, M. Viale, V. Zdravkovic, *Empirical investigation of starling flocks: a benchmark study in collective animal behaviour*, Animal Behaviour 76,1, 201-2015 (2008), DOI:10.1016/j.anbehav.2008.02.004.

[3] A. Baskaran, M. C. Marchetti, *Hydrodynamics of self-propelled hard rods*, Journalref: Phys. Rev. E Vol. 77, 031311 (2008), arXiv:0708.2401.

[4] A. Baskaran, M. C. Marchetti, *Statistical mechanics and hydrodynamics of bacterial suspensions*, Proceedings of the National Academy of Sciences, Vol. 106, pp 15567-15572, DOI:10.1073/pnas.0906586106.

[5] S. Bazazi, F. Bartumeus, J. J. Hale, I. D. Couzin, *Intermittent Motion in Desert Locusts: Behavioural Complexity in Simple Environments*, PLoS Comput Biol 8(5): e1002498, DOI:10.1371/journal.pcbi.1002498.

[6] E. Bertin, M. Droz, G. Guillaume, *Hydrodynamic equations for self-propelled particles: microscopic derivation and stability analysis*, J. Phys A: Math. Theor. 42, 445001 (2009), arXiv:0907.4688.

[7] E. Bertin, M. Droz, G. Guillaume, *Boltzmann and hydrodynamic description for self-propelled particles*, Phys. Rev. E 74, 022101 (2006), arXiv:cond-mat/0601038.

[8] E. Bertin, A. Baskaran, H. Chaté, M. C. Marchetti, *Comparison between Smoluchowski and Boltzmann approaches for self-propelled rods*, submitted to Phys. Rev. E (July 2015), arXiv:1507.07812.

[9] L. Boltzmann, *Weitere Studien über das Wärmegleichgewicht unter Gasmolekülen*, Wiener Bericht, 66, 275-370, 1872.

[10] H. Chaté and F. Ginelli, G. Gregoire, f. Raynaud, *Collective motion of self-propelled particles interacting without cohesion*, Phys. Rev. E 77, 046113 (2008), DOI:10.1103/PhysRevE.77.046113.

[11] H. Chaté, F. Ginelli, R. Montagne, *Simple model for active nematics: quasi-long-range order and giant fluctuations*, Phys. Rev. Lett. 96, 180602 (2006), DOI:10.1103/PhysRevLett.96.180602.

[12] I. D. Couzin, J. Krause, *Self-Organization and Collective Behavior in Vertebrates*, Advances in the Study of Behavior 32, 1–75 (2003), DOI:10.1016/S0065-3454(03)01001-5.

[13] M. Cross and H. Greenside, *Pattern Formation and Dynamics in Nonequilibrium sytems*, Cambridge University Press, 2009.

[14] J. Deseigne, O. Dauchot, and H. Chaté, *Collective Motion of Vibrated Polar Disks*, Phys. Rev. Lett. 105, 098001 (2010), arXiv:1004.1499.

[15] J. Deseigne, O. Dauchot, and H. Chate, *Vibrated polar disks: spontaneous motion, binary collisions, and collective dynamics*, Soft Matter, 2012,8, 5629-5639, arXiv:10.1039/C2SM25186H.

[16] P. G. de Gennes and J. Prost, *The Physics of Liquid Crystals*, Clarendon Phys. Rev. Ess, Oxford 1993.

[17] J. Denk, *Formation of Macroscopic Order in Systems of Self-Propelled Particles for Different Collision Rules*, Ludwig Maximilians Universität, München (June 2013)

[18] H.P. Erickson, D.E. Anderson, M. Osawa, *FtsZ in bacterial cytokinesis: cytoskeleton and force generator all in one*, Microbiol Mol Biol Rev. 2010 Dec;74(4):504-28., DOI:10.1128/MMBR.00021-10.

[19] F. D. C. Farrell, M. C. Marchetti, D. Marenduzzo, and J. Tailleur, *Pattern Formation in Self-Propelled Particles with Density-Dependent Motility*, Phys. Rev. Lett. 108, 248101 (2012), DOI:10.1103/PhysRevLett.108.248101.

[20] F. Ginelli, F. Peruani, M. Bär, H. Chaté, *Large-scale collective properties of self-propelled rods*, Phys. Rev. Lett. 104, 184502 (2010), DOI:10.1103/PhysRevLett.104.184502.

[21] F. Ginelli and H. Chaté, *Relevance of Metric-Free Interactions in Flocking Phenomena*, Phys. Rev. Lett. 105, 168103 (2010), DOI:10.1103/PhysRevLett.105.168103.

[22] G. Gregoire, H. Chaté, *Onset of collective and cohesive motion*, Physical Review Letters 92, 2 (2004) 025702, arXiv:cond-mat/0401208.

[23] G. Gregoire, H. Chaté, Y. Tu, *Moving and staying together without a leader*, Physica D 181 (2003) p. 157-170, arXiv:cond-mat/0401257.

[24] Guttal, V., Romanczuk, P., Simpson, S.J., Sword, G.A. & Couzin, I.D., *Cannibalism as a driver of the evolution of behavioral phase polyphenism in locusts*, Ecology Letters 15, 1158-1166, DOI:10.1111/j.1461-0248.2012.01840.x.

[25] T. Ihle, *Invasion-wave-induced first-order phase transition in systems of active particles*, Phys. Rev. E 88, 040303(R)-2013, DOI:10.1103/PhysRevE.88.040303.

[26] T. Ishikawa, G. Sekiya, Y. Imai, T. Yamaguchi, *Hydrodynamic Interactions between Two Swimming Bacteria*, Biophys. Journal 93 , 6 , 2217 - 2225 (2007), DOI:10.1529/biophysj.107.110254.

[27] Y. Katz, K. Tunstrøm, C. C. Ioannou, C. Huepe, and I. D. Couzin, *Inferring the structure and dynamics of interactions in schooling fish*, PNAS 2011 108 (46) 18720-18725, DOI:10.1073/pnas.1107583108.

[28] E. Lauga and T. R. Powers, *The hydrodynamics of swimming microorganisms*, Rep. Prog. Phys. 72 096601(2009), DOI:10.1088/0034-4885/72/9/096601.

[29] M. C. Marchetti, J.-F. Joanny, S. Ramaswamy, T. B. Liverpool, J. Prost, Madan Rao, R. Aditi Simha, *Hydrodynamics of soft active matter*, Rev. Mod. Phys. 85, 1143 (2013), DOI:10.1103/RevModPhys.85.1143.

[30] A. M. Menzel, *Collective motion of binary self-propelled particle mixtures*, Phys. Rev. E 85, 021912 (2012), arXiv:1202.0792.

[31] N. D. Mermin and H. Wagner, *Absence of Ferromagnetism or Antiferromagnetism in One- or Two-Dimensional Isotropic Heisenberg Models*, Phys. Rev. Lett. 17, 1133 (1966), DOI:10.1103/PhysRevLett.17.1133.

[32] S. Mishra, A. Baskaran, M. C. Marchetti, *Fluctuations and Pattern Formation in Self- Propelled Particles*, Phys. Rev. E 81, 061916 (2010), DOI:10.1103/PhysRevE.81.061916.

[33] S. Mishra, K. Tunstrøm, I. D. Couzin, C. Huepe, *Collective dynamics of self-propelled particles with variable speed*, Phys. Rev. E 86, 011901(2012), DOI:10.1103/PhysRevE.86.011901.

[34] V. Narayan, S. Ramaswamy, N. Menon, *Long-lived Giant Number Fluctuations in a Swarming Granular Nematic*, Science 317, 105 (2007), arXiv:cond-mat/0612020.

[35] F. Peruani, F. Ginelli, M. Bär, H. Chaté, *Polar vs. apolar alignment in systems of polar self-propelled particles*, J. Phys.: Conf. Ser. 297, 012014 (2011), arXiv:1302.0267.

[36] F. Peruani, A. Deutsch, M. Baer, *A mean-field theory for self-propelled particles interacting by velocity alignment mechanisms*, Eur. Phys. J. Special Topics 157, 111 (2008), arXiv:0806.2475.

[37] A. Peshkov, E. Bertin, F. Ginelli and H. Chaté, *Boltzmann-Ginzburg-Landau approach for continuous descriptions of generic Vicsek-like models*, Eur. Phys. J Special Topics 223, 1315 (2014), arXiv:1404.3275.

[38] A. Rabani, Gil Ariel, and A. Be'er, *Collective Motion of Spherical Bacteria*, PLoS One. 2013; 8(12): e83760, DOI: 10.1371/journal.pone.0083760.

[39] S. Ramaswamy, *The Mechanics and Statistics of Active Matter*, Ann. Rev. Cond. Matt. Phys. 1, 301 (2010), arXiv:1004.1933.

[40] E. Rauch, M.Millonas, and D. Chialvo, *Pattern formation and functionality in swarm models*, Phys. Lett. A 207, 185 (1995), DOI:10.1016/0375-9601(95)00624-C.

[41] G. S. Redner, A. Baskaran, M. F. Hagan, *Reentrant Phase Behavior in Active Colloids with Attraction*, Phys. Rev. E 88, 012305 (2013), arXiv:1303.3195.

[42] P. Romanczuk, I. D. Couzin, and L. Schimansky-Geier, *Collective Motion due to Individual Escape and Pursuit Response* , Phys. Rev. Lett. 102, 010602 (2009), DOI:10.1103/PhysRevLett.102.010602.

[43] V. Schaller, C. Weber, C. Semmrich, E. Frey and A.R. Bausch, *Polar Patterns of driven Filaments*, Nature 467, 73-77 (2010), arXiv:10.1038/nature09312.

[44] V. Schaller, C. Weber, C. Semmrich, E. Frey and A.R. Bausch, *Polar pattern formation: hydrodynamic coupling of driven filaments*, Soft Matter, 2011,7, 3213-3218, DOI:10.1039/C0SM01063D.

[45] D. Sinkovits, *Flocking Behavior*, tech. rep., University of Illinois at Urbana-Champaign, United States, 2006.

[46] S. H. Strogatz, *Nonlinear Dynamics and Chaos: With Applications to Physics, Biology, Chemistry, and Engineering (Studies in Nonlinearity)*, Perseus Books Group, 1994.

[47] F. Thüroff, C. A. Weber, E. Frey, *Numerical Treatment of the Boltzmann Equation for Self-Propelled Particle Systems*, Phys. Rev. X 4, 041030 (2014), arXiv:1411.4544.

[48] F. Thüroff, C. A. Weber, E. Frey, *A Critical Assessment of the Boltzmann Approach for Active Systems*, Phys. Rev. Lett. 111, 190601 (2013), arXiv:1310.5234.

[49] F. Thüroff, C. A. Weber, E. Frey, *Snake-Solving numerically active kinetic equations*, Submitted for publication.

[50] J. Toner, Y. Tu, *Flocks, herds, and schools: A quantitative theory of flocking*, Phys. Rev. E 58, 4828 (1998), arXiv:cond-mat/9804180.

[51] J. Toner, Y. Tu, *Long-Range Order in a Two-Dimensional Dynamical XY Model: How Birds Fly Together*, Phys. Rev. Lett. 75, 4326 – Published 4 December 1995, DOI:10.1103/PhysRevLett.75.4326.

[52] J. Toner, Y. Tu, S. Ramaswamy, *Hydrodynamics and phases of flocks*, Annals of Physics 318 (1), 170-244 (2005), DOI:10.1016/j.aop.2005.04.011.

[53] D. Tong, *Kinetic Theory*, University of Cambridge Graduate Course, Michaelmas Term 2012, http://www.damtp.cam.ac.uk/user/tong/kinetic.html.

[54] T. Vicsek, A. Czirok, E. Ben-Jacob, I. Cohen, O. Sochet, *Novel type of phase transition in a system of self-driven particles*, Phys Rev Lett. 75(6):1226-1229 (1995), arXiv:cond-mat/0611743.

[55] T. Vicsek, A. Zafeiris, *Collective Motion*, Physics Reports 517, pp. 71-140, 2012, arXiv:1010.5017.

[56] C. A. Weber, T. Hanke, J. Deseigne, S. Léonard, O. Dauchot, E. Frey, H. Chaté, *Long-range Ordering of Vibrated Polar Disks*, Phys. Rev. Lett. 110, 208001 (2013), DOI:10.1103/PhysRevLett.110.208001.

[57] C. A. Weber, F. Thüroff, E. Frey, *Role of particle conservation in self-propelled particle systems*, New J. Phys. 15, 045014 (2013), arXiv:1301.7701.

[58] H. H. Wensink, V. Kantsler, R. E. Goldstein, and J. Dunkel, *Controlling active self-assembly through broken particle-shape symmetry*, Phys. Rev. E 89, 010302(R), 2014, DOI:10.1103/PhysRevE.89.010302.

[59] H. P. Zhang, Avraham Be'er, E.-L. Florin, and Harry L. Swinney, *Collective motion and density fluctuations in bacterial colonies*, Proc Natl Acad Sci U S A. 2010 Aug 3; 107(31): 13626–13630, DOI:10.1073/pnas.1001651107.